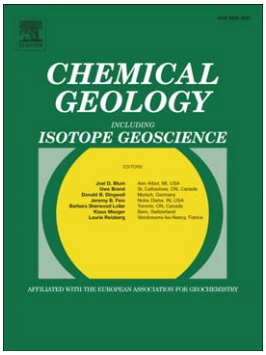

The Pretty Hill Formation as a natural analogue for CO_2 storage; An investigation of mineralogical and isotopic changes associated with sandstones exposed to low, intermediate and high CO_2 concentrations over geological time

K.E. Higgs, R.R. Haese, S.D. Golding, U. Schacht, M.N. Watson

PII: S0009-2541(14)00459-8
DOI: doi: 10.1016/j.chemgeo.2014.10.019
Reference: CHEMGE 17384

To appear in: *Chemical Geology*

Accepted date: 20 October 2014

Please cite this article as: Higgs, K.E., Haese, R.R., Golding, S.D., Schacht, U., Watson, M.N., The Pretty Hill Formation as a natural analogue for CO_2 storage; An investigation of mineralogical and isotopic changes associated with sandstones exposed to low, intermediate and high CO_2 concentrations over geological time, *Chemical Geology* (2014), doi: 10.1016/j.chemgeo.2014.10.019

The Pretty Hill Formation as a natural analogue for CO_2 storage; an investigation of mineralogical and isotopic changes associated with sandstones exposed to low, intermediate and high CO_2 concentrations over geological time.

K.E. Higgs[1,2], R.R. Haese[1,3], S.D. Golding[1,4], U. Schacht[1,5], M.N. Watson[1]

[1]CRC for Greenhouse Gas Technologies (CO2CRC), GPO Box 463, Canberra, ACT 2601, Australia.

[2]GNS Science, 1 Fairway Drive, Avalon, Lower Hutt, New Zealand.

[3]The Peter Cook Centre for CCS Research and School of Earth Sciences, University of Melbourne, Melbourne, Victoria 3010, Australia.

[4]The University of Queensland, Brisbane, Queensland 4072, Australia.

[5]The University of Adelaide, Adelaide, South Australia 5005, Australia.

Tel +64 4 570 1444, Fax +64 4 570 4600

Corresponding author: Karen Higgs. Email: k.higgs@gns.cri.nz

ABSTRACT

The Pretty Hill Formation of the Otway Basin (Australia) has been studied as a natural analogue for geological storage of anthropogenic CO_2 in order to examine the effects that CO_2 concentration and reservoir heterogeneity have on CO_2-related reactions. New petrographic data are presented, which validate the use of Hylogger™ as a tool to investigate high-resolution vertical changes in reservoir mineralogy. The integrated data set confirms earlier interpretations, showing that chlorite has been altered to kaolinite and siderite/ankerite in reservoir facies exposed to moderate and high CO_2 concentrations, while chlorite remains the dominant clay mineral in all parts of the formation where CO_2 content is low.

Differences have been observed in the degree of CO_2-related reaction relative to CO_2 concentration and reservoir heterogeneity. Where CO_2 content is very high (c. 98 mol%) and associated with high water saturations, both chlorite and detrital feldspars have undergone complete reaction in the reservoir facies, resulting in quartzose sandstones with a kaolinite matrix, and with siderite as the dominant carbonate precipitate. Conversely, where CO_2 content is moderate (c. 29-57 mol%) and within the gas leg of the reservoir, chlorite has undergone significant reaction, but much of the original feldspar is preserved, suggesting relatively minor reaction. Carbonate cements from the moderate CO_2 gas-leg comprise calcite, siderite and ankerite, occurring as cemented zones

associated with rock heterogeneities and the present-day gas-water contact. Heterogeneities within the gas-leg are likely to have associated pore fluid contacts, whereby relatively high water saturations will be present in the fine-grained baffles and seals. The most advanced feldspar reaction occurs locally at the contact between baffles and reservoir rock, while reactions have been significantly impeded in the finer grained units due to their low permeabilities.

Stable isotope data presented for carbonate cements analysed from wells with low and moderate CO_2 levels show no clear distinction. Relatively early formed calcite has $\delta^{13}C$ values that require an organic carbon source, suggesting precipitation unrelated to the reservoir CO_2 in the Otway Basin. In contrast, diagenetically late calcite and siderite samples display two distinct $\delta^{13}C$ groups (dependent on carbonate type), where the calculated fluid carbon isotope compositions are similar to documented magmatic CO_2 reservoired in the nearby Caroline Field. This suggests that magma-derived CO_2 may have been more prevalent through the Pretty Hill Formation than previously thought. Although the CO_2 has not been contained over the long term in the low CO_2 sites, it may have caused the local dissolution of carbonate and laumontite cement, and also contributed a source of carbon for late-stage calcite cements.

These studies illustrate the importance of understanding both the reservoir composition and vertical heterogeneity of potential storage systems. Fluid-mineral reactions are likely to be advanced within stacked reservoir facies and impeded within siltstone layers, while the distribution of carbonate cement may increase reservoir heterogeneity by the formation of cemented siltstone/sandstone layers, thereby creating impermeable barriers or baffles to CO_2.

Keywords: carbon dioxide, CO_2-related reactions, Hylogger, natural analogue, stable isotopes, CO_2 reservoirs, Otway Basin

1. INTRODUCTION

Carbon capture and storage (CCS) involves capturing anthropogenic CO_2 and storing it underground in geological formations in an attempt to reduce greenhouse gas levels in the atmosphere. In certain areas, naturally occurring CO_2 already occurs in the subsurface, locally contained within accumulations, and these can be regarded as geological analogues of potential storage sites. By studying the composition and textural/diagenetic alteration of rocks within these natural analogues and by understanding the types of reactions that have occurred, it is possible to provide long-term predictions of what fluid-rock reactions can be expected when CO_2 is injected into a subsurface storage site. Such studies also allow us to test and validate modelling assumptions and respective outcomes. For example, the carbon trapping mineral dawsonite ($NaAlCO_3(OH)_2$) is commonly

predicted to precipitate under CO_2 storage conditions, yet this mineral is only rarely found in naturally CO_2-rich reservoirs (e.g., Hellevang et al., 2011). Using data from natural analogues, we are able to estimate the amount and type of mineral dissolution and precipitation likely to occur on a case-by-case basis, thereby addressing issues such as storage potential, injectivity and storage method, all of which are essential to successful implementation of CCS technologies (e.g., Gaus, 2009).

The importance of natural analogues to CCS have been recognised for a long time and several studies have been undertaken (e.g., Baines and Worden, 2004; Golding et al., 2013; Haszeldine et al., 2005; Higgs, 2011; Higgs et al., 2012; Kampman et al., 2013; Moore et al., 2005; Pearce et al., 1996; Stevens et al., 2003; Uysal et al., 2011; Watson et al., 2004a, 2004b; Wilkinson et al., 2009). Typically, natural analogue sites, similar to many hydrocarbon fields, have been characterised following analysis of a few representative samples that are usually taken from the main reservoir facies. This work has been vital to our understanding of potential storage sites. However, there remains a need to understand whether the types and degree of CO_2-related reactions differ within any single reservoir interval, potentially resulting in variable dissolution and/or precipitation that could be beneficial or detrimental to injectivity or storage. In this paper we attempt to answer some of these questions by integrating data from traditional analytical techniques with some newer techniques such as Hylogger™ and QEMSCAN®.

Our study has focussed on the Lower Cretaceous Pretty Hill Formation, which is a producing hydrocarbon reservoir in several fields of the Otway Basin, in southern Australia (Fig. 1). Gas accumulations within the Pretty Hill Formation have highly variable CO_2 contents from <1 mol% to >90 mol%, making it a very attractive and arguably unique natural analogue. In addition, the formation has been well characterised by numerous earlier petrographic studies (e.g., Alexander, 1992; Little and Phillips, 1995; Martin and Baker, 1993; Phillips, 1991; Watson et al., 2004a, 2004b), and several cores have been recently analysed using Hylogger™ by the Australian Government, thereby opening up a new data source.

2. GEOLOGICAL BACKGROUND

2.1 Basin History

The Otway Basin is an extensional basin that developed along the southern margin of eastern Australia, with sedimentation initiated in the Late Jurassic and continuing through to the Tertiary-recent (Von Der Borch et al., 1970). It forms part of the Southern Rift System associated with the

late Australia/Antarctica stage break-up of the Gondwana super-continent (Perincek and Cockshell, 1995). The basin is bound to the north by the Padthaway Ridge granite complex and extends southwards into the Great Australian Bight. About 25% of the basin is located in the state of South Australia, 50% in the State of Victoria, and 25% in the State of Tasmania (Fig. 1).

In the Late Jurassic, NE-SW extension resulted in the formation of a narrow, SE-trending, half graben along what is now the northern margin of the Otway Basin, including the Penola and Ardonachie troughs. In the east, the half graben (Gellibrand Trough) failed and during the Early Cretaceous a much larger rift developed to the south, extending into the Gippsland and Bass basins (Geological Survey of Victoria, 1995).

Rifting ceased in the mid-Cretaceous, and slow seafloor spreading and formation of oceanic crust began between Australia and Antarctica, marking the breakup and beginning of drifting. The whole area was subject to uplift, with a basin-wide unconformity occurring at the top of the Cretaceous (Von Der Borch et al., 1970). Subsequently the Port Campbell Embayment and other regions began to subside southeast of the Warrnambool High. In Middle Eocene time, the rate of seafloor spreading south of Australia increased and there was a strong pulse of NW-SE compression, resulting in NE-trending folds, faults and reactivation of earlier structures (Geological Survey of Victoria, 1995), and the development of two further well defined unconformities (Von Der Borch et al., 1970).

2.2 Basin Stratigraphy

The Jurassic Casterton Formation comprises the oldest sediments penetrated in the Otway Basin to date and probably represent the earliest basin fill. They comprise interbedded shales and volcaniclastic material deposited in a low energy fluvial-lacustrine environment (Baker and Skinner, 1999).

The overlying Lower Cretaceous Crayfish Group (forming the basal part of the Otway Supergroup; Fig. 2) was also deposited during rifting as episodic movement accommodated crustal extension. It includes the Pretty Hill Formation, deposited as predominantly fluvial facies within fault-bounded depocentres (Cockshell et al., 1995; Parker, 1992), and overlying siltstones and mudstones of the Laira Formation. The area was subject to rapid burial through most of the Early Cretaceous with high associated heat flow (Duddy, 1997). The area was relatively stable through the latter part of the Early Cretaceous, resulting in the deposition of a thick succession of fine-grained clastics (Eumeralla Formation).

Widespread uplift and erosion occurred in the mid-Cretaceous, which has been attributed to the onset of sea floor spreading (Baker and Skinner, 1999). The Late Cretaceous Sherbrook Group was

deposited on the resulting unconformity (Fig. 2), comprising a condensed sandstone succession onshore and a deltaic system offshore (Morton, 1990). The top of the Sherbrook Group is marked by the basin-wide, top-Cretaceous unconformity, and is overlain by Tertiary sandstones and claystones of the Wangerrip Group deposited onshore in a fluvial-deltaic setting (Gravestock et al., 1986). Fossiliferous limestones of the Heytesbury Group overlie a Late Eocene unconformity and were deposited as a prograding marine sequence up to the top of the Miocene (Fig. 2). Volcanic activity was widespread in the eastern part of the basin through the Tertiary and into recent times, possibly related to basin subsidence (Von Der Borch et al., 1970).

2.3 Early Cretaceous Petroleum System

The Lower Cretaceous Pretty Hill Formation represents the main petroleum producing reservoir system of the Otway Basin. The overall depositional environment for the Pretty Hill Formation is considered to be fluvial, comprising both braided and meandering stream facies (Cockshell et al., 1995; Parker, 1992), although there is some evidence locally for marine influence (Sagasco Resources Ltd., 1992). Reservoir sandstones of the Pretty Hill are sealed by the overlying Laira Formation, which, based on empirical data, suggests good seal quality (Boult, 1997) demonstrated by the lowest cap seal risk of the Penola Trough (Jones et al., 2000).

Producing hydrocarbon fields, prospects and leads within the Crayfish Group of the Penola Trough are all bound by a series of complex planar en-echelon faults (Jones et al., 2000) that are directly related to oblique syn-depositional rifting and display a dominant NW-SE and less prominent E-W strike (Lovibond et al., 1995). Hydrocarbon accumulations have been discovered on both footwall and hangingwall sides of major dislocation planes, yet most have relatively small, confined trap capacities (< 100 BCF; Lovibond et al., 1995). Producing areas include the Katnook, Ladbroke Grove, Haselgrove, Haselgrove South and Redman fields (Fig. 1), with several non-commercial gas wells, and numerous wells with paleogas columns (e.g., Zema-1) or residual oil (e.g., Redman-1; Boult and Hibburt, 2002). Biomarker data suggests multiple source rocks for the various oils, condensates and bitumens of the Pretty Hill Formation, but with gas probably originated from *in situ* intra-Pretty Hill shale (Padley et al., 1995).

The main risk factors to hydrocarbon discovery within the Late Cretaceous petroleum play are structural integrity and small targets (Boult and Hibburt, 2002), with evidence for hydrocarbon leakage from several structures in the basin resulting from fault reactivation (Jones et al., 2000; Lyon et al., 2005). In the Otway Basin, there is also a risk of reservoir depletion by late CO_2 charge, with CO_2 contents ranging from <1 mol% in parts of the Penola Trough to >90 mol% in the Gambier and Port Campbell Embayments (e.g., Burns, 1992; Mulready, 1977). Isotope analysis from the

commercial Caroline CO_2 field (Fig. 1) in the Late Cretaceous Waarre Formation (98 mol% CO_2) has shown that this CO_2 is of magmatic origin (Chivas et al., 1987), while age-dating and qualitative evidence suggests late timing of CO_2 charge, within the last 1 My (McDougall et al., 1966; Sheard, 1995), suggesting migration via fault systems and associated with Plio-Pleistocene volcanics (Boult and Hibburt, 2002; Chatfield, 1992; Fig. 2). Boult et al. (2004) have suggested that a cross fault seal has prevented CO_2 migration into the central part of the Penola Trough resulting in the locally occurring low CO_2 gas fields (Katnook, Redman, Hazelgrove; Fig. 1).

2.4 Petrographic Characterisation of the Pretty Hill Formation

Numerous petrographic studies have been undertaken on the Pretty Hill Formation, many of which were contracted by oil companies to assess reservoir quality (e.g., Alexander, 1992; Little and Phillips, 1995; Martin and Baker, 1993; Phillips, 1991). More recently, a comparative study was undertaken by Watson (Watson et al., 2004a, 2004b; Watson, 2012) to specifically address how CO_2 has affected reservoir rocks of the Otway Basin.

The Pretty Hill reservoir sandstones are shown to predominantly comprise fine- to medium-grained, moderately to well sorted lithic arenites. Diagenetic alteration is reported to include albitisation of feldspar grains, chloritisation of volcanic rock fragments, grain-coating clay minerals, minor authigenic quartz, and local cementation by kaolinite ($Al_2Si_2O_5(OH)_4$), calcite ($CaCO_3$), dolomite-ankerite ($Ca(Fe,Mg,Mn)(CO_3)_2$), siderite ($FeCO_3$) and laumontite ($Ca(AlSi_2O_6)_2\ 4H_2O$) (e.g., Alexander, 1992; Little and Phillips, 1995; Martin and Baker, 1993; Phillips, 1991; Watson et al., 2004a, 2004b).

Differences in the type and abundance of detrital and authigenic minerals within the Pretty Hill Formation have been noted by several authors and attributed to different CO_2 concentrations within the reservoir. Watson et al. (2004a, 2004b) have suggested that sandstones from low CO_2 sites represent sandstone compositions prior to late CO_2-charge, with a key feature of these sandstones being the extensive chlorite and chlorite-smectite grain coatings. Conversely, sandstones from high CO_2 sites have been interpreted to represent CO_2-altered sandstone compositions whereby Na-plagioclase feldspar (albite, $NaAlSi_3O_8$), volcanic rock fragments, chlorite and calcite, are variably replaced by authigenic quartz, kaolinite and ferroan carbonates (Watson et al., 2004a, 2004b).

3. STUDY OBJECTIVES

This study aims to use and integrate various analytical techniques in order to better understand CO_2-related reactions within the Late Cretaceous Pretty Hill Formation, and in particular to investigate

the effect that CO_2-concentration and reservoir heterogeneity have on CO_2-water-rock reactions. Key objectives of the study are to:

1. Assess the application of Hylogger™ and QEMSCAN® data to complement established petrographic methods particularly in regards to representing gradual and abrupt changes in lithology.
2. Assess differences in the mineral composition from a single formation exposed to low, intermediate and high CO_2 concentrations to assist in the interpretation of reaction pathways and conditions.

These studies should provide insights into how CO_2-induced diagenesis will vary within a single reservoir interval over geological time, and will provide inputs to geochemical models. In this way, predictions can be made for the likely short- and long-term reactions associated with CO_2 storage, the effect these reactions have on porosity and permeability, and the implications for both storage potential and injectivity. This work is vital for selection of storage sites and modelling the behaviour of CO_2 in the subsurface.

4. METHODOLOGY

Four wells have been investigated as part of this study, chosen on the basis of CO_2 content and data availability. Redman-1 and Zema-1 are low CO_2 wells (<1 mol% CO_2) located in the Penola Trough, approximately 2.5 km and 10 km northwest (respectively) of the Katnook Gas Field (Fig. 1). Ladbroke Grove-3 is a producing gas reservoir, also located in the Penola Trough, approximately 1 km to the south of Katnook, and with moderately high CO_2 recovered from the produced gas (c. 29-57 mol% CO_2; Simeone and Mitchell, 2001). Garvoc-1 is a very high CO_2 well (c. 98 mol% CO_2) located approximately 250 km to the SW in the Port Campbell Embayment (Fig. 1). Conventional cores are available through part of the Pretty Hill Formation in all four wells, with Redman-1 core taken from the gas-leg, Zema-1 and Garvoc-1 core from the paleo gas-leg, and Ladbroke Grove-3 core taken through the gas-water contact (GWC); Hylogger data is available for the cores from Redman-1, Zema-1 and Ladbroke Grove-3 (Table 1).

4.1 Hylogger Interpretation

Hylogging™ is a new technique that has been developed by CSIRO to provide rapid, non-invasive, non-destructive and statistically-robust mineral spectroscopy. It combines a variety of sensitive reflectance spectrometers covering the Visible-Near InfraRed (VNIR), Short-Wave InfraRed (SWIR), and Thermal InfraRed (TIR) wavelengths, with robotic sample handling and semi-automated

interpretation software (The Spectral Assistant, TSA™) to provide continuous, semi-quantitative mineralogical information at the cm-scale (Huntington et al., 2010). Many minerals have spectral signatures that can be detected in this spectral range (Table 2).

Hylogger data (Hylogger-3) were provided for three of the study wells by the State of South Australia and these data loaded into TSA™ Viewer software for data interpretation (version 7.1.0.051). TSA™ (Berman et al., 1999) is a general unmixing algorithm that advises the most likely dominant and secondary spectrally active minerals in each spectrum, their relative weights and an error measure (standardised residual sum of squares; Huntington et al., 2010). TSA™ is based on a trained data set of approximately 500 "pure" reflectance spectra for commonly-occurring minerals, and consequently will not identify relatively rare mineral species. TSA™ abundances are relative spectral fitting fractions that sum to 1 for the number of minerals that are reported.

Spectral data are recorded every 25 mm and these high-resolution data have been examined in our study to investigate vertical changes in the relative proportion of different clay minerals and carbonate cements. Previous validation work of TIR Hylogger data suggests that they can be successfully correlated with X-ray Diffraction (XRD), X-ray Fluorescence (XRF) and microprobe data (Cudahy et al., 2009). However, little work has been reported on the VNIR and SWIR wavelength data. Further details on the Hylogging technique can be found in Huntington et al. (2010).

4.2 Petrographic Analysis

A range of petrographic techniques have been applied to the study of core and cuttings samples from the four study wells (Table 3). Samples from low and moderate CO_2 wells were primarily selected on the basis of the Hylogger response in order to assess Hylogger data and investigate changes in the mineralogy related to reservoir heterogeneities and the GWC. In the moderate CO_2 well (Ladbroke Grove-3), the sampling was biased towards sandstones where the clay mineralogy apparently deviated from being kaolinite-dominated; kaolin-rich sandstones have been well characterised and interpreted in other studies (e.g., Watson et al., 2004a, 2004b). Samples from the high CO_2 well were selected primarily to investigate the authigenic mineralogy of the short core, and also to compare the mineralogy of cuttings from the top sandstone/base seal boundary with that from cuttings in the basal part of the formation.

A list of analytical techniques that have been undertaken on core and cuttings samples is provided in Table 3 with methods detailed below. All sample depths referred to in this paper are measured depth below kelly bushing (MDKB) unless otherwise stated.

4.2.1 Thin Section Petrography

Thirty-four core samples were analysed using transmitted light microscopy on impregnated and stained thin sections (thin sections stained for K-feldspar and carbonate), with eight samples from Garvoc-1, fourteen from Ladbroke Grove-3, eight from Zema-1 and four from Redman-1 (Table 3). Impregnation was undertaken in a vacuum to remove gas from the samples. The samples were dried at 50°C and the epoxy cured at 40°C. Modal point-count analysis was undertaken on 30 samples to investigate grain size recording the long axis of each grain (100 counts per section of silt size or above) and mineralogy/porosity (300 counts per section); the remaining four samples were qualitatively examined to further investigate changes close to the GWC at Ladbroke Grove-3 (Table 3). Data are summarised in Tables 4 and 5.

4.2.2 Scanning Electron Microscopy (SEM)

SEM analysis was undertaken on selected core chip samples from all four study wells (Table 3) using a Phillips XL30 FEG-SEM located at Adelaide Microscopy, University of Adelaide. Samples were presented as freshly broken, platinum coated blocks mounted on aluminium stubs, and imaging was carried out using operating conditions of 15-20 kV and spot size 3-4 microns. This work was undertaken to provide additional information on pore-system geometry, morphology of authigenic minerals, and paragenetic relationships.

4.2.3 QEMSCAN

Automated mineral, particle- and pore-size analysis was undertaken on 12 core and 16 cuttings samples using an SEM fitted with four light element X-ray energy dispersive spectrometer detectors (QEMSCAN®, model Zeiss EVO 50 series). Sixteen samples were analysed from Garvoc-1, three from Zema-1, and nine from Ladbroke Grove-3 (Table 3). The QEMSCAN system measures and identifies minerals within a sample, allowing for fast, quantitative and repeatable mineralogical and rock texture analyses. Full details of the method are provided in Gottlieb et al. (2000), Pirrie et al. (2004) and Allen et al. (2012).

QEMSCAN analysis was undertaken on impregnated and carbon-coated polished thin sections or polished blocks (core and cuttings samples respectively) using a vertical and horizontal pixel spacing of 10 µm. Mineral identification, mapping and advanced data analysis were performed by the iDiscover™ software suite licenced by FEI™. Bulk mineralogy was calculated by the software for all analysed samples (Table 6); particle size was calculated for all quartz particles in the bulk sample based on stereologically corrected grain size grouped into Wentworth classes by the iDiscover™ software.

Ditch cutting samples were subdivided into a number of lithotypes in order to capture the variability in mineralogical composition and lithological texture observed within the sample set (Table 7). Particle categorisers were devised to subdivide the cuttings lithologies based upon quartz grain size and area percent calculations of the various mineral phases within each cutting. Bulk mineralogy was then generated for each lithotype. The software was also used to produce a "map" of mineral types and sediment textures across the scanned sample area.

4.2.4 X-ray Diffraction (XRD)

Semi-quantitative X-ray diffraction (XRD) analysis was undertaken on a subset of the thin section core samples (Table 3). The samples were first prepared by crushing and grinding in a Rocklabs swing mill using a Tungsten Carbide grinding head. Powders were then scanned on a Bruker D4 Diffractometer, from 5° to 70° 2θ, in 0.020° steps at 1 second per step, using a Cu anode X-ray tube. Minerals were identified using Bruker Eva Diffracplus V3 software, and Bruker Topas software was used to quantify the minerals. Results are summarised in Table 8.

4.3 Stable Isotope Analysis

Carbon and oxygen isotope analyses have been undertaken on samples from the studied wells and are discussed along with pre-existing data. The selection of samples for isotopic analysis was based on the distribution of carbonate in core; significant cements (>5 %) were not observed through the cored interval at Garvoc-1, and are relatively rare in the Ladbroke Grove-3 well. In total, 11 samples were selected for carbon and oxygen isotopic analysis (Table 3). Most samples are dominated by a single phase authigenic carbonate, but four samples from Ladbroke Grove-3 contain two carbonate phases, grain-coating siderite/ankerite and pore-filling calcite. Carbonate mineralogy was determined by thin section analysis, XRD, and in some cases QEMSCAN.

The carbonates were reacted off-line with orthophosphoric acid to extract CO_2 for carbon and oxygen isotope analysis (McCrea, 1950). Calcite was reacted at 25^{o}C for 1 day and siderite at 75^{o}C for three days. A differential extraction method was used for samples that contained both calcite and siderite, where the sample was first reacted at 25^{o}C for 2 hours prior to gas take off (calcite fraction). The sample was then returned to the 25^{o}C water bath for the remainder of the day before being returned to the extraction line where CO_2 liberated through the day was pumped away. Finally, the sample was placed in a 75^{o}C water bath for 3 days (siderite fraction). Sample gases were analysed on an Isoprime Dual Inlet Stable Isotope Ratio Mass Spectrometer in the Stable Isotope Geochemistry Laboratory at the University of Queensland. Stable isotope analyses are reported in per mil (‰) relative to V-SMOW for oxygen and V-PDB for carbon (Table 9), with analytical

uncertainties better than ± 0.1 ‰ (1σ) based on replicate analyses of international (NBS-18 and NBS-19) and in-house standards.

5. RESULTS

5.1 Low CO_2 Wells (Redman-1, Zema-1)

5.1.1 Core Summary

Logs and core images show the upper part of the cored interval at Redman-1 (2825-2837.5 m core depth) to comprise stacked sandstones with one thin siltstone bed (c. 0.5 m thick); the lower part of the core is composed of a fairly thick (c. 3 m) siltstone-dominated interval, underlain and overlain by the more typical reservoir sandstone facies (Fig. 3). Parts of the lower sandstone unit are heavily stained by residual hydrocarbons (black in core). By comparison, the entire 54 m cored interval at Zema-1 (2412.5-2466.3 m core depth) is composed of stacked reservoir sandstones with only very thin (mm-scale) siltstone laminae (Fig. 4).

5.1.2 Hylogger Summary

Thermal infrared (TIR) data for both wells suggest that in most cases quartz is the dominant mineral over the cored intervals and that feldspar, mostly plagioclase, is also common. Smectite is identified at this wavelength over the siltstone-dominated interval at Redman-1 (Fig. 3); TIR data suggest that smectite is overall more common in Zema-1, particularly towards the top of the cored interval (Fig. 4). Carbonate (siderite) has been identified as a subordinate component at a few depths in both wells.

The short-wave infrared (SWIR) spectra suggest that white mica and chlorite are the dominant two hydrous mineral groups over most of the cored intervals (Figs. 3 & 4), where muscovite, phengite and lesser muscovitic illite and phengitic illite are the white mica minerals, and Fe-chlorite is the main chlorite species. In most cases, smectite (e.g., montmorillonite) has not been detected by the SWIR, or occurs as subordinate phases over discrete horizons in Zema-1 (Fig. 4). However, below 2458 m log depth (2454 m core depth) in Zema-1, smectite, particularly palygorskite is relatively more abundant. Carbonate has been identified as a minor component in both wells at similar depth intervals to the TIR data, but in most cases the carbonate identified by SWIR is calcite, with rare ankerite and siderite detected. Epidote is the only other minor mineral detected by the SWIR.

Notably parts of the core that are very dark (i.e., the thick siltstone interval and the hydrocarbon-stained interval at Redman-1) are aspectral in terms of the SWIR (null values). The visible-near infrared (VNIR) spectra are also predominantly aspectral and therefore yield little useful information

from the two low CO_2 cores. VNIR data locally suggests the presence of sulphates, and iron oxides, particularly in the upper part of the Zema-1 core.

5.1.3 Petrographic Summary

Samples are generally comparable from the two low CO_2 wells in terms of their ranges of textures and compositions. Sandstones comprise fine- to medium-grained, typically moderately well sorted lithic feldsarenites and feldspathic litharenites (Table 4, Fig 5). Framework grains are dominated by monocrystalline quartz and feldspar with common, but subordinate lithic fragments. The abundance of feldspar varies significantly, being notably low in the three upper samples from Zema-1 (Tables 5, 8 & Fig. 5); feldspar is mostly plagioclase and displays evidence of minor dissolution and locally albitisation. Lithic fragments mostly comprise variably degraded and clay-replaced volcanic clasts (see below).

Authigenic clay minerals are variably abundant, being most common in poorly cemented sandstones where they comprise thick grain-rimming coatings. These clays are principally chlorite or chlorite-smectite (Table 8) occurring as an early tangential grain-coating followed by thicker radial grain-coatings; chlorite, smectite, together with minor albite, also occur as replacement phases of volcanic lithic fragments. Other grain-replacement clay minerals are also common (Table 5), and comprise illite, illite-smectite and minor intermixed kaolinite (Table 8).

Carbonate cements are locally pervasive in the cores from Redman-1 and Zema-1, mostly occurring as non-ferroan to slightly ferroan calcite with a sparry or less common poikilotopic habit. Minor amounts of authigenic quartz, and rare dolomite and siderite have also been observed. Laumontite is a local cement phase in Zema-1, occurring in the petrographic samples at 2459.95 m and 2465.75 m (core depths), while residual hydrocarbons have been identified in trace amounts in a few samples, and are a significant part of one sample from Redman-1 (2841.65 m core depth).

5.1.4 Integration of High-Resolution Hylogger and Petrography Data

High-resolution Hylogger data suggest that clay minerals are predominantly Fe-chlorites with subordinate illite/muscovite/phengite over much of the sandstone cored intervals (e.g., Fig. 6A, 6B & 7A). However, thin zones locally occur where chlorite has not been detected by Hylogger and where the spectral data record illite/mica as the dominant clay type (e.g., Figs 6C & 7B). There are no clearly defined clay-mineral profiles observed on the high-resolution spectral logs.

Petrographic data confirms the presence of relatively chlorite-rich zones and chlorite-poor zones. In most cases, the chlorite-poor zones are associated with low volumes of total clay, relatively low volumes of total feldspar, and high concentrations of carbonate cement (e.g. Figs 6C & 7B). Other

examples where chlorite has not been identified from the high-resolution spectral data are over siltstone/mudstone intervals (mm- and cm-scale siltstone laminae or rip-up siltstone clasts), and where the core is visibly stained by residual hydrocarbons (i.e., basal part of Redman-1 core). In both these cases, chlorite has been confirmed as a minor component from petrographic studies, with relatively poorly crystallised illitic clay being dominant.

In addition to the above, palygorskite is locally the only clay mineral picked up by high-resolution Hylogger through the basal part of the Zema-1 core. However, petrographic studies show that chlorite (as probable chlorite-smectite) does occur in significant amounts through these intervals (Fig. 7C). It is therefore likely that the mineral identified as palygorskite by Hylogger is actually the grain-coating clay observed in thin section and SEM.

Laumontite was observed in thin section as a patchy cement near the base of the cored interval (Table 5), yet has not been detected by Hyloggyer. Notably, however, the core linescan from these intervals displays a characteristic mottled, diagenetic fabric, and it is suggested that this fabric is a result of the patchy laumontite cementation .

5.1.5 Stable Isotope Data

Carbon and oxygen isotopic compositions were determined for one calcite sample from Redman-1 (repeat analysis run for this sample) and two calcite samples from Zema-1 (Table 9, Figure 8). The Redman-1 sample is from the gas-leg of the reservoir and has $\delta^{18}O$ and $\delta^{13}C$ values of 0.2 to 0.3 ‰ and -6.5 to -6.2 ‰, respectively. The Zema-1 samples have $\delta^{18}O$ and $\delta^{13}C$ values from 1.8 to 3.3 ‰ and -7.3 to -6.8 ‰, respectively (Table 1).

5.2 Moderate CO_2 Well (Ladbroke Grove-3)

5.2.1 Core Summary

The core linescan image for Ladbroke Grove-3 shows that the Pretty Hill Formation comprises thick stacked sandstone facies (Fig. 9), similar to that observed at Redman-1 and Zema-1. Siltstones occur throughout the cored interval at the mm-scale (as lamination), as thin beds (c. 0.5 m thick, e.g., 2527 m log depth), and as one thicker (c. 3.5 m) siltstone-dominated interval (e.g., 2533-2536 m log depth).

5.2.2 Hylogger Summary

Thermal infrared (TIR) data show a fairly similar response to that observed in the low CO_2 cores (compare Fig. 9 with Figs 3 and 4). Quartz is the dominant mineral identified over these wavelengths; feldspar (plagioclase with subordinate microcline) is only locally dominant over quartz.

White micas (illite) and smectite have been detected from the TIR data over specific horizons of the cored interval, and are generally associated with fine-grained interbeds. These clays are also apparently associated with higher feldspar/lower quartz detection. Carbonate (siderite) is a very minor component identified by the TIR data.

The short-wave infrared (SWIR) spectra from Ladbroke Grove-3 cores are very different to that recorded from the low CO_2 cores (Redman-1 and Zema-1). SWIR suggest that kaolin minerals are dominant down to approximately 2570 m log depth (2566.5 m core depth), which is the approximate GWC (Fig. 9); chlorite has not been detected over this interval. White mica (mostly muscovite and illitic muscovite) is common, particularly in the upper part of the interval, while both mica and smectites (montmorillonite) are dominant over discrete horizons that correspond to clay-rich intervals (Fig. 9).

Below 2570 m (log depth), there is a distinct change in reflectance spectroscopy to predominantly mica, smectite, and chlorite; these spectra are more comparable to the profiles recorded at Redman-1 and Zema-1 (compare bottom part Fig. 9 with Figs 3 and 4). SWIR data suggests that micas in this lower interval are mostly paragonitic illite with lesser muscovite and phengite, smectites are mostly montmorillonite with local palygorskite, and chlorite is Fe-rich.

Carbonate (calcite, ankerite, siderite) and epidote have been identified by the SWIR as minor components at a few depths over the cored interval, and are mostly associated with smectite-rich horizons and the GWC.

The visible-near infrared (VNIR) spectra are predominantly aspectral at Ladbroke Grove-3 and therefore are of limited value for mineral identification.

5.2.3 Petrographic Summary

The petrographic samples analysed from Ladbroke Grove-3 are texturally similar to those from Redman-1 and Zema-1, mostly comprising fine- to medium-grained, moderately well sorted lithic feldsarenites (Table 4, Fig. 5). The detrital mineralogy is also similar, with framework grains dominated by monocrystalline quartz and feldspar (mostly plagioclase) with common, but subordinate lithic fragments (mostly volcanics). Total feldspar content is highly variable in the samples from Ladbroke Grove-3, with the highest feldspar contents occurring in the uppermost and lowermost cored interval (i.e. above siltstone baffles and below GWC, Figs 5 and 9). Both feldspars and some lithic clasts from Ladbroke Grove-3 locally display evidence of dissolution and local albitisation.

The authigenic clay mineralogy documented by Watson et al. (2004b) and others for typical sandstones from the Ladbroke Grove Field is significantly different to that observed at low CO_2 sites. Kaolinite was recorded as the main clay phase in these earlier studies and has also been observed as a common authigenic mineral in this present study, although other clays are locally dominant (Tables 5, 6 & 8).

Kaolinite has been observed as very fine, grain-lining clays, as variably sized plates and books within primary and secondary pores, and as a replacement mineral of chloritised grains. Illite and illite-smectite is common in the Ladbroke Grove-3 samples, and mostly occurs as a grain-replacement phase. Chlorite (including chlorite-smectite) is only a minor component of most samples, but has been observed in similar amounts to the low CO_2 wells in all samples from below the present-day GWC (Table 5).

Carbonates are variably abundant at Ladbroke Grove-3, but in comparison to the low CO_2 wells they are mostly composed of Fe/Mg-rich phases (siderite/ankerite) occurring as replacement minerals of detrital feldspar and grain-coating chlorite; these Fe/Mg carbonates have not been identified in the two samples from the lower part of the core (Table 5). Pore-filling and grain-replacement calcite is locally pervasive in the petrographic samples, occurring as both a slightly ferroan sparry phase and a non-ferroan poikilotopic phase. Other authigenic minerals include minor pore-filling quartz overgrowths, which commonly display a prismatic habit; notably dawsonite, a carbon trapping mineral predicted to precipitate under CO_2 storage conditions (cf. Hellevang et al., 2005; Worden, 2006), was not identified in samples from Ladbroke Grove-3.

5.2.4 Integration of High Resolution Hylogger and Petrography Data

Hylogger data from the cored interval at Ladbroke Grove-3 can be subdivided into several intervals, each with distinct clay mineralogy.

Above the siltstone-dominated interval (2533-2536 m log depth; cf. Fig. 9), the spectral data indicate that kaolinite is common within sandstone lithologies, but that it may also be co-dominant with illite or montmorillonite (Fig. 10). Montmorillonite is reported as the dominant clay where the sandstones contain thin interbeds or mudstone laminae and/or where they are cemented by carbonates (Fig. 10). In some cases, there appear to be slight trends in kaolinite intensity, increasing towards the top and base of reservoir-baffle contacts, which has been confirmed through petrographic data (e.g., Fig. 10). Through more homogenous sandstone intervals, kaolinite is often the only clay mineral species identified by Hylogger (e.g., see Fig. 8 & lower interval Fig. 11A); petrographic analyses have confirmed that kaolinite is indeed the dominant authigenic clay mineral but that other clay minerals are also present.

Below the siltstone-dominated interval (cf. Fig. 9) but above 2566.5 m (core depth; 2570 m log depth), Hylogger data infer thick intervals of sandstone with spectra picking up kaolinite as the only clay mineral (e.g., Fig. 11A). Over some intervals the spectral intensity of kaolinite is lowered slightly in response either to where carbonate cement is detected (e.g., Fig. 11B), or where thin muddy laminae containing minor illite/muscovite are detected. In some cases, the carbonate cements are too minor to be picked up by the spectral data but they have been observed from the core linescan (e.g., as siderite mottling), and these zones have locally been validated by petrographic analysis. A relationship between montmorillonite and lithology is apparent, similar to that observed in the overlying cored interval.

Below 2566.5 m (core depth; 2570 m log depth; approx. GWC), the high-resolution Hylogger data records a change from kaolinite- and montmorillonite-dominated clay (above 2566.5 m) to montmorillonite- and chlorite-dominated clay (below 2566.5 m). Petrographic analyses confirm the presence of chlorite-dominated clay in this lower part of the cored interval (e.g., Fig 11c). There is very little detection of carbonates within this lower cored interval, although a fairly thick cemented zone is apparent at the change in clay mineralogy (Fig. 9).

5.2.5 Stable Isotope Data

Carbon and oxygen isotopic compositions were determined for eight pore-filling calcite samples (repeat analysis run for four of these samples) and four grain-coating siderite samples from Ladbroke Grove-3 (Table 9, Fig. 8).

Three calcite samples from the gas-leg of the reservoir above 2565.0 m (core depth) have $\delta^{18}O$ and $\delta^{13}C$ values from 0.8 to 2.3 ‰ and –7.5 to -6.3 ‰, respectively. A fourth sample from the gas-leg contains calcite (Calcite I) with a comparable $\delta^{18}O$ value but very different $\delta^{13}C$ value (2.1 and -12.1 ‰ respectively). Siderites measured from two samples from the gas-leg of the reservoir have $\delta^{18}O$ and $\delta^{13}C$ values from 3.6 to 7.2 ‰ and -4.7 to -2.4 ‰, respectively.

Two calcite samples taken close to the GWC (2565.67-2566.58 m core depth) and two calcite samples from the water-leg of the reservoir below 2566.58 m (core depth) have overlapping $\delta^{18}O$ and $\delta^{13}C$ values from 3.6 to 5.1 ‰ and -6.9 to -5.2 ‰, respectively. Siderites analysed from the two samples from near the GWC have $\delta^{18}O$ and $\delta^{13}C$ values from 7.3 to 7.6 ‰ and -2.5 to -2.0 ‰, respectively.

In the moderate CO_2 well, calcite is invariably depleted in ^{18}O and ^{13}C relative to siderite where they occur together in the same sample (Table 9). The data also clearly demonstrate a change in calcite $\delta^{18}O$ values with depth, where samples below 2565.0 m (core depth; GWC and water-leg on Fig. 8)

are several per mil higher than those above this depth (gas-leg on Fig. 8). Calcite $\delta^{13}C$ values on the other hand are very similar apart from one sample at 2523.05 m (core depth) and do not show any trends with depth or gas saturation.

5.3 High CO_2 Well (Garvoc-1)

5.3.1 Core Summary

A short (4m long) core was recovered from near the top of the Pretty Hill Formation at Garvoc-1. It comprises stacked medium-grained to pebbly sandstones with local mudstone rip-up clasts and some evidence of cross bedding. The sandstones have a distinctive white clay matrix but otherwise appear similar to the other Pretty Hill cores and are most likely of fluvial origin.

5.3.2 Core Petrography

The core from Garvoc-1 is principally composed of medium-grained, moderately well sorted sublitharenites (Table 4, Fig 5). As such, the present-day (diagenetically modified) detrital mineralogy is different to that of samples analysed from the Penola Trough. Framework grains are predominantly monocrystalline quartz, feldspar is virtually absent and lithic fragments are a minor component (mostly volcanics).

The reservoir sandstones at Garvoc-1 are remarkable in that they contain large amounts of authigenic clay (Fig. 12), which has given the distinctive white colouration to the core. Kaolinite is the dominant authigenic clay mineral (Tables 5 & 6), occurring as very fine, grain-coating clays, as variably sized plates and books within primary and secondary pores, and with a significant volume as a grain replacement phase. Other authigenic clay minerals include relatively minor illite-smectite, which mostly occurs as a grain-replacement phase. Chlorite and smectite are virtually absent.

Carbonate cements form a fairly minor authigenic phase in the Garvoc-1 core and are mostly Fe-rich phases (siderite/ankerite); calcite has not been identified from thin section or SEM. Authigenic quartz is ubiquitous in the core samples but is also a relatively minor phase. Dawsonite was not identified in this high CO_2 well.

5.3.3 Cuttings Petrography

Cuttings analysed above and below the cored interval show more variability in both lithology and mineralogy compared to the Garvoc-1 core (Tables 6 & 7). Lithotyping confirms the wellsite ditch cuttings descriptions, showing that siltstones are dominant in the upper 3 analysed samples from the top Pretty Hill Formation and that sand (i.e., loose grains) or sandstone is dominant in the

remaining cuttings intervals (Fig. 12). The relative abundance of siltstone cuttings varies between samples and demonstrates the locally interbedded nature of the Pretty Hill Formation.

Loose sand grains (quartz) are very common in the Garvoc-1 cuttings; these grains are most likely to have been derived from sandstones similar to those observed in the cored interval, suggesting that the fines (i.e., any clay matrix) have been washed away. This will have affected the bulk mineralogy data, which shows that the cuttings are predominantly quartz (Table 6). The high loose grain component is an indication that the sandstones are poorly consolidated/cemented, which is most likely due to the relatively shallow burial depth at this wellsite (i.e. no high temperature diagenetic reactions; <100°C, Duddy, 1997).

In comparison, the bulk mineralogy of sandstone cuttings is relatively comparable to the core mineralogy, with sandstones dominated by quartz but with common kaolinite and locally significant carbonate. Carbonates are mostly iron-rich phases (siderite/ankerite) but with calcite becoming relatively common at the top of the formation (Fig. 12). The slightly lower clay content of sandstone cuttings compared to core samples is most likely a reflection of the small cuttings size (most comprising only a few grains). Feldspar is a very minor component of the sandstone cuttings and chlorite is virtually absent.

Bulk mineralogy of the siltstone cuttings show lower quartz content compared to the sandstone cuttings, associated with slightly higher feldspar, kaolinite, chlorite, illite/mica and carbonate (Fig. 12). It is also notable that both the sandstone and siltstone cuttings show an increase in calcite and ankerite towards the top of the Pretty Hill Formation at Garvoc-1 with more vertical variability shown by the siderite profile.

6. DISCUSSION

6.1 Validation of Hylogger Data

Hylogger spectra (TIR, SWIR and VNIR) have been examined and compared with thin section, XRD, SEM and QEMSCAN data. In most cases the dominant minerals (quartz and plagioclase feldspar) identified by TIR, and the dominant clay minerals (chlorite, illite/mica, kaolinite) identified by SWIR have been validated by the more traditional mineralogical techniques (e.g., Figs 6, 7, 10, 11). As such, the profiles of TSA^{TM} abundances are considered a useful measure of changes in the relative proportion of quartz, feldspar and clay mineralogy. These data are discussed in the following sections in terms of how they relate to the degree of diagenetic alteration.

Two of the main limitations with Hylogger data are that absolute values are not measured and that the technique does not pick up small quantities of some minerals. This has been particularly noticeable for carbonate phases and subordinate clay mineral species (e.g., Figs 6B, 10, 11A & C). Additionally, in cases where the dominant clay has been identified by thin section, SEM and/or QEMSCAN to be smectite-rich (i.e. chlorite-smectite), the Hylogger technique appears to only have detected smectite. Further work is recommended to address some of these issues.

6.2 Mineral Paragenesis

Watson et al. (2004a, 2004b) have suggested that the diagenetic evolution of the Pretty Hill Formation can be subdivided into two periods, corresponding to pre-CO_2 influx and post-CO_2 influx paragenesis, whereby the CO_2 relates to a late (Plio-Pleistocene) source from the Newer Volcanics (Fig. 2). They suggest that sandstone mineralogy from the low CO_2 Katnook Field is equivalent to the pre-CO_2 reservoir mineralogy at the moderate CO_2 Ladbroke Grove Field, and with authigenic phases comprising chlorite, calcite, albite and laumontite. In contrast, late phase CO_2-related reactions were interpreted to have only occurred in the higher CO_2 Ladbroke Grove Field, whereby feldspars, lithics and chlorites reacted, resulting in precipitation of authigenic kaolin, quartz and locally carbonate (e.g., Watson et al., 2004a, 2004b). The main late-stage CO_2-related net-reactions have been summarised by Watson et al. (2004b) and Watson (2012) as follows:

$Fe_5Al_2Si_3O_{10}(OH)_8 + 10CO_2 + 3H_2O = 5FeCO_3 + Al_2Si_2O_5(OH)_4 + SiO_2 + 2H^+ + 5HCO^-_3(aq)$

Fe chlorite water siderite kaolinite quartz bicarbonate (Eq. 1)

$2NaAlSi_3O_8 + 3H_2O + 2CO_2 = Al_2Si_2O_5(OH)_4 + 4SiO_2 + 2NaHCO_3(aq)$

albite water kaolinite quartz sodium bicarbonate (Eq. 2)

$2CaNaAl_3Si_5O_{16} + 7H_2O + 4CO_2 = 3Al_2Si_2O_5(OH)_4 + 4SiO_2 + 2CaCO_3 + 2NaHCO_3(aq)$

Ca/Na plag water kaolinite quartz calcite sodium bicarbonate (Eq. 3)

$2KAlSi_3O_8 + 3H_2O + 2CO_2 = Al_2Si_2O_5(OH)_4 + 4SiO_2 + 2KHCO_3(aq)$

K-feldspar water kaolinite quartz potassium bicarbonate (Eq. 4)

$Ca_4[Al_8Si_{16}O_{48}].16H_2O + 4CO_2 = 4CaCO_3 + 4Al_2Si_2O_5(OH)_4 + 8SiO_2 + 8H_2O$

laumontite calcite kaolinite quartz water (Eq. 5)

Paragenetic observations from this present study are discussed for samples from the low (Redman-1, Zema-1), moderate (Ladbroke Grove-3), and high (Garvoc-1) CO_2 sites below, and in many cases

are consistent with earlier interpretations (e.g., Duddy, 1986; Little and Phillips, 1995; Watson et al., 2004a, 2004b).

6.2.1 Grain-Coating Chlorite/Smectite

In most sandstones from the Pretty Hill Formation there is evidence to suggest that Fe-rich chlorite was the most pervasive early authigenic mineral (e.g., Figs 6, 7, 11), occurring as a grain-rimming phase and replacing unstable grains. The preservation of extensive chlorite grain-coatings exclusively in the low CO_2 wells and below the GWC in the moderate CO_2 well is evidence that alteration of grain-coating chlorite to ankerite/siderite and kaolinite was a late diagenetic reaction in response to high concentrations of CO_2 (Equation 1 above). Paragenetic relationships show that chlorite precipitated before hydrocarbon migration and prior to the main phases of kaolinite, quartz and carbonate cementation.

Smectites appear most commonly associated with fine-grained facies and are thus related to depositional environment (e.g., Figs 3 & 9). However, in several cases, smectite has also been identified from Hylogger and petrographic data (QEMSCAN, SEM) in the sandstones. In most of these cases the smectite occurs as a grain-coating phase and probably represents a mixed-layer chlorite-smectite clay mineral. It is unclear whether the smectite formed during early diagenesis as a mixed-layer chlorite-smectite clay, or if it represents a partial replacement of precursor grain-coating chlorite, or both. It is likely that the presence of smectite may be partly related to degradation and alteration of volcanic lithic clasts and/or volcanic glass.

6.2.2 Kaolinite and Quartz

The relative abundance of authigenic kaolinite and quartz in samples from the high CO_2 well and above the GWC in the moderate CO_2 well is evidence that these are relatively late-stage mineral phases that formed in response to high CO_2 resident within the reservoir over a period of geological time (Equations 1-4 above). The morphology and distribution of kaolinite (product of CO_2-reactions) as micro-crystalline grain-coating and booklet secondary pore-filling clays is consistent with replacement of chlorite and feldspar precursors respectively. In addition, paragenetic relationships from samples at both the moderate and high CO_2 wells show that authigenic quartz is commonly intergrown with kaolinite, suggesting co-genetic precipitation.

6.2.3 Calcite Cement

Calcite is the dominant carbonate phase in both low CO_2 cores (Figs 3 & 4), occurring as rare poikilotopic cement and more common sparry calcite. These are interpreted to be texturally similar to the Calcite I^W and II^W phases (respectively) identified as pre-CO_2 cements described in the Katnook

Field by Watson et al. (2004a[1]), where Calcite I^W predates Calcite II^W. In our study a further late-stage, poikilotopic calcite cement has been identified in the moderate CO_2 well (Calcite III), which may be equivalent to late-stage calcite described by Watson et al. (2004a) in the Waarre Sandstone of the Caroline CO_2 field (Calcite III^W).

Calcite I is relatively minor in our study wells, but where present it is interpreted as a relatively early carbonate phase, with grains displaying only minor grain-coating clays, and little mechanical compaction prior to cementation. This phase shows some evidence for enclosure of minor chlorite and authigenic quartz and has undergone some dissolution, possibly as a result of the late-stage (magmatic) CO_2 migration.

Calcite II is interpreted as a later diagenetic phase observed in the low and moderate CO_2 wells. The calcite is locally observed to replace thick grain-coating chlorite, and also locally pseudomorphs laumontite cement (e.g., Fig. 6). These observations suggest formation after development of extensive clay coats and after zeolite cementation, and are therefore later than that described by Watson for Calcite II^W in the Katnook Field (Watson et al., 2004a). The evidence implies a relatively late-stage carbon source, possibly from thermal maturation of the source rocks (prior to hydrocarbon migration), or associated with displacement and degradation of paleo-oil by gas, or potentially from late-stage (Plio-Pleistocene) magmatic CO_2.

Calcite III is interpreted as the latest calcite phase. It encloses all other authigenic mineral phases, including thick siderite rims, which are interpreted as pseudomorphs of grain-coating chlorite. The occurrence of these cements close to the GWC at Ladbroke Grove-3 together with late-stage paragenesis, is consistent with formation associated with the present-day reservoired CO_2 (e.g., Equation 3 above).

6.2.4 Siderite/Ankerite

Minor siderite observed in low CO_2 wells is interpreted as an early cement phase (referred to here as Siderite I). It is commonly associated with detrital clay and organic matter, and is interpreted to represent precipitation close to the sediment-water interface. Siderite I has also been interpreted in minor amounts in the moderate CO_2 well.

A second, later phase of siderite/ankerite is interpreted in the moderate and high CO_2 wells (Siderite II, equivalent to Siderite I^W of Watson et al., 2004a). In both wells, micritic/micro-spar siderite clearly replaces grain-coating clays (e.g., Fig. 11A) and thus developed relatively late in the

[1] The superscript W after carbonate phases, e.g., Calcite I^W refers to phases identified by Watson et al. (2004a), which are not necessarily equivalent to the carbonate phases identified in this study.

diagenetic history. Coarser cement also occludes porosity, having developed after or coincident with feldspar dissolution, suggesting it is a replacement mineral of feldspar grains, and showing a progressive change from siderite to ankerite precipitation.

Siderite II (described here) is interpreted to have formed as CO_2-rich fluids reacted with chlorite and feldspars in moderate and high CO_2 wells (e.g., Equation 1 above). Where Siderite II and calcite occur together in Ladbroke Grove-3, the former is invariably the earlier phase. Feldspar is a more stable phase than chlorite, as demonstrated by the presence of feldspars and almost complete reaction of chlorite in the moderate and high CO_2 wells. This provides an explanation for the sequence of carbonate formation post-CO_2 charge where grain-rimming and pore-filling siderite precipitation (Siderite II) was followed by late stage calcite cementation (Calcite III). The fluids initially would have been acidic but likely evolved to near neutral pH as a result of mineral buffering. This may indicate that siderite formed across a range of pH conditions as the fluid composition evolved in response to late CO_2 reactions, whereas the calcites are interpreted to have formed under near neutral to alkaline conditions. These results are consistent with modelling work undertaken by Kirste et al. (2004).

6.2.5 Laumontite Cement

Salt and pepper textures, identified as laumontite, have been noted in several Pretty Hill cores (e.g., Watson et al., 2004b; Duddy, 1986; Sagasco Resources Ltd., 1992). In most cases, laumontite has been identified in low CO_2 wells (e.g., throughout wells Katnook-2 and -3; Watson et al., 2004b, and in the lower part of the Zema-1 core; this study). However, laumontite was also identified below the GWC in the moderate CO_2 well Ladbroke Grove-1 (2710-2720 m; Watson et al., 2004b).

Petrographic evidence from Zema-1 indicates that the laumontite cement formed during burial diagenesis as a post-chlorite, pore-filling and feldspar-replacement phase (e.g., Fig. 7C). Previous studies suggest that the zeolite probably formed between 100-130 °C as a result of the alteration of volcanic glass (e.g., Phillips, 1991) or feldspar albitisation (e.g., Duddy, 1986). However, given its very high solubility, the amount of laumontite that was originally precipitated is uncertain.

Watson et al. (2004b) suggests that all laumontite above the GWC in Ladbroke Grove-1 was dissolved in the presence of the late CO_2 charge to form authigenic calcite, kaolinite and quartz (Equation 5 above). Zema-1 is a low CO_2 well, but given the lack of trap and the CO_2-prone nature of the Otway Basin, it is possible that CO_2 may also have migrated through the reservoir at Zema-1 and resulted in the dissolution of laumontite. The distribution of laumontite at the base of Zema-1 may reflect a paleo-GWC whereby laumontite has been dissolved through the paleo gas-leg.

6.2.6 Hydrocarbon and Associated CO_2 Migration

The presence of residual hydrocarbons in both low CO_2 cores shows that liquid hydrocarbons migrated into the reservoirs prior to the present-day gas/condensate charge. Based on thermal modelling at Katnook-2, Lovibond et al. (1995) predicted hydrocarbon migration occurred in the mid Cretaceous after a period of rapid burial and therefore long before CO_2 charge from the Newer Volcanics. Paragenetic relationships show residual hydrocarbons enclosing grain-coating clays and pre-dating poorly-ferroan calcite spar cement (Calcite II) and quartz cements (2841.65 m, Redman-1). This suggests that oil migration post-dated grain-coating chlorite but pre-dated the formation of Calcite II and some authigenic quartz.

The release of CO_2 from thermal maturation of source rocks will have occurred prior to oil migration (e.g., Burnham and Sweeney, 1989; Surdam et al., 1984), and it is possible that CO_2 from this origin may have circulated through the Pretty Hill reservoirs resulting in some mineral diagenesis. However, given the significant differences in authigenic mineralogy between the moderate/high CO_2 sites and the low CO_2 site (where CO_2 has been sourced from late Plio/Pleistocene magma), most of the CO_2-related reactions (Equations 1-5 above) are considered to be unrelated to an earlier CO_2 charge event.

The present-day gas/condensate charge is thought to be a fairly late-stage and possibly on-going charge associated with the maturation of intra-formational source rocks.

6.3 Late CO_2 Reactions and CO_2 Concentration

Results from our study suggest that the degree of CO_2-related reaction is greatest in the well with very high present-day CO_2 concentrations, and least in the two wells with very low present-day CO_2 concentrations.

Detrital feldspar was one of the main mineral reactants proposed by Watson et al. (2004a, 2004b) in the Pretty Hill Formation, and dissolution textures observed in this study in the moderate CO_2 well, together with secondary pore-filling kaolinite are both consistent with CO_2-related diagenesis (Equations 2-4 above). In addition, the presence of locally abundant feldspar in both low and moderate CO_2 wells and virtual absence in the high CO_2 well (Fig. 5) is consistent with more advanced CO_2-related diagenesis where CO_2 contents are very high, and indicates that overall the feldspar reactions are fairly sluggish.

It is possible that the original composition of sandstones from Garvoc-1 (high CO_2 well) may have been different to those in the Penola Trough, and as such there may have been fewer of the mineral

reactants. This is difficult to assess given the scarcity of penetrations at this level. Certainly there will have been different depositional histories for these rocks within the half grabens and these sandstones will not be correlatable to other sub-basins (Parker, 1995). However, the presence of feldspars within fine-grained cuttings at Garvoc-1 and absence in the sandstone core (Table 6, Fig. 13), together with the occurrence of common secondary pore-filling kaolinite, implies that feldspars were originally present in this high CO_2 well and therefore that they have undergone more complete reaction than feldspars at Ladbroke Grove-3 (moderate CO_2 well).

Despite the broad trends in feldspar abundance, it is clear that the amount of feldspar is highly variable in low and moderate CO_2 wells, and this suggests that there are factors other than present-day CO_2 content that are controlling feldspar abundance. It is suggested here that some of the feldspar variability might be a response to stratigraphic variations in the paleo-pore fluid chemistry that have resulted in locally enhanced feldspar reaction, possibly associated with carbonate cementation or fluids associated with paleo-oil migration (Fig. 5).

Chlorite is considered the other main mineral reactant in the Pretty Hill Formation (Watson et al., 2004a, 2004b), and the virtual absence of chlorite in either the high or moderate CO_2 (above GWC) core samples suggests that in both wells chlorite has undergone almost complete reaction. Given the significant distance between the low/moderate and high CO_2 wells, there is some uncertainty as to how much chlorite was originally present in the latter. However, the core contains very abundant kaolinite (product of CO_2-related diagenesis), which together with the common micro-crystalline grain-coating habit and traces of chlorite (Fig. 12), is consistent with replacement of a chlorite precursor. In addition, thin section descriptions from Woolsthorpe-1 (a well located approximately 20 km to the WNW of Garvoc-1) report locally significant chlorite (Geological Survey of Victoria, 1995), which would be consistent, at least locally, for chlorite-rich sandstones within the Pretty Hill Formation in this region. It is therefore suggested that chlorite has undergone almost complete reaction in reservoirs with CO_2 concentrations ranging from moderate to high (29-98 mol%), and is preserved in reservoirs with low CO_2 concentrations (<0.1 mol%).

A further indication of how CO_2 concentration affects reactions is illustrated at Ladbroke Grove-3, where the CO_2 concentration in the gas decreases upwards from the GWC to the top of the reservoir (Fig. 9). Hylogger data from stacked reservoir facies at the top of the gas-leg (above the siltstone-dominated interval 2533-2536 m log depth) detect lower proportions of kaolinite and carbonates (products of reaction) compared to the reservoir facies in the lower part of the gas-leg. This difference might be a response to lower CO_2 contents in the upper interval (i.e. CO_2 is being sequestrated as a mineral phase as it passes through the reservoir), or possibly lower residence

times as the CO_2 breaches the intraformational baffle (i.e. CO_2 has entered at the base of the field and the baffle has impeded flow/diffusion). Chlorite has not been detected in this upper interval, and petrographic observations provide evidence for alteration of grain-coating clays to Siderite II and kaolinite. This might suggest that the lower kaolinite/carbonate values within the upper gas-leg are a result of less advanced feldspar reactions rather than less advanced chlorite reaction, which would be supportive of greater chlorite reactivity compared to feldspar reactivity. This is consistent with relatively high feldspar abundances in the upper cored interval (upper gas-leg) as measured by point-counting (Fig. 5).

Despite our observations, it is notable that there are many other wells in the Otway Basin that have only undergone partial CO_2 reaction progress whilst within near 100% CO_2 (Watson, 2012). This demonstrates that factors other than present-day CO_2 concentration are important in driving the reactions, particularly the amount of CO_2 dissolving into solution, driven by anion saturation levels.

6.4 Late CO_2 Reactions and Reservoir Heterogeneities

Examination of high-resolution spectral logs, together with conventional logs and petrographic data, show that the degree of CO_2-related reactions is related to lithology. The most obvious examples of this are where the reservoir sandstones are interbedded with siltstone baffles. A change in clay mineralogy is associated with these baffles in low CO_2 wells from chlorite-illite/mica (sandstones) to smectite-illite/mica (baffles, e.g., Figs 3 & 9), demonstrating a facies control on clay mineralogy (e.g., Fig. 3). A similar response is shown by the moderate CO_2 well where the clay mineralogy changes from kaolinite-illite/mica (i.e. reacted sandstone) to dominantly smectite-illite/mica (baffle). It is suggested here that the relatively high smectite content and low kaolinite content of the baffles in the moderate CO_2 well is evidence for significantly impeded reaction in the finer grained units.

Within the reservoir facies, data suggest that most complete reaction (chlorite to kaolinite) has occurred in moderate and high CO_2 wells within the thickly stacked sandstones compared to more interbedded lithologies (e.g., Fig. 9, 12). Additionally, high-resolution Hylogger data suggests that the most advanced feldspar reaction has occurred in the coarsest sandstones (i.e., top of the upward-coarsening packages). As such, the degree of reaction (measured by the amount of kaolin) is locally greatest at the contact between baffles and reservoir rock (e.g., Fig 10). This observation is generally supported by numerical simulations of mineral reactions within bedded systems (e.g., Xu et al., 2005; Dirk Kirste pers. comm. 2013), which show that much reaction (dissolution and precipitation) occurs close to lithological boundaries.

Results also indicate that the distribution of carbonate cements is related to reservoir heterogeneities. In the moderate CO_2 well, carbonates tend to be concentrated in zones adjacent to lithology boundaries and also close to the present-day GWC (Fig. 9). In the high CO_2 well, carbonate cements are observed to increase up to the top reservoir/seal boundary (Fig. 12). The lithology boundaries can be considered to be the sites of intra-formational fluid contacts, whereby higher water saturation (Sw) will be present in the fine-grained baffles and seals and where CO_2-rich fluids diffuse into the low-permeability rocks (refer to discussion below).

6.5 Late CO_2 Reactions and the Gas-water Contact

Core samples from Ladbroke Grove-3 (moderate CO_2 well) have been examined to investigate differences in diagenetic reactions that have occurred across the GWC. Results from this study show that chlorite has largely been replaced by kaolinite in the gas-leg of this well, but with preservation of chlorite in the underlying water-leg (below 2569 m core depth; Fig. 9). It is suggested here that the sandstones below the GWC largely represent unreacted rock, which is generally consistent with formation water chemistry. Watson et al. (2004b) have shown that high bicarbonate (HCO_3^-) concentration characterises the formation water from Ladbroke Grove-1 above the GWC, which most likely represents residual water saturated with CO_2; below the GWC the major ion composition of water is not significantly different from that in CO_2 poor fields (Katnook-2 and -3).

We propose that the change in bicarbonate concentration in formation water above and below the GWC is the likely reason for carbonate cementation close to this boundary and also adjacent to intra-formational contacts within the gas-leg (resulting from reservoir-baffle/seal contacts). In all cases these contacts will represent differences in PCO_2 from high (in the reservoir) to relatively low (in baffles, seals, and below the CO_2-water contact). The deposition of carbonate minerals is likely to occur as the CO_2 diffuses into clay-rich caprocks containing reactive phyllosilicate minerals (Gherardi et al., 2007; Xu et al., 2005) and is converted to carbonate minerals according to Equation 1.

There are some complexities in facies and clay mineralogy at the GWC in Ladbroke Grove-3 that need to be better understood. The clay mineralogy changes from kaolinite-illite/mica within coarse-grained basal sandstones, to illite/mica-smectite or illite/mica-chlorite within underlying, finer-grained sandstones (Fig. 11). Given the presence of alternating chlorite- and smectite-rich zones at the top of the water-leg at Ladbroke Grove-3 (c. 1-2 m thick zones), it is recommended that further work is undertaken to address this, determine the lateral continuity of the layers and investigate whether smectite (as opposed to kaolinite) could perhaps represent an alteration product of CO_2-rich fluids over very specific zones (e.g., close to the GWC). This could potentially be in response to a palaeo-GWC, which has been advocated for the Ladbroke Grove Field by Lyon et al. (2004), whereby

partial leakage of hydrocarbons (c. 9 m palaeocolumn, Little, 1996) may have occurred up the fault periodically during fault reactivation.

Despite the uncertainties regarding the timing of smectite formation, it is suggested here that the clear change in clay mineralogy below the GWC (c. 2570 m log depth), and the carbonate cements that are concentrated close to this boundary, are related to pore-fluid composition. As mentioned, it is likely that the GWC has moved over time with leakage of gas/CO_2 up faults. However, the structures in the Penola Trough are often described as filled to spill and we therefore suggest that the present-day contact has not changed significantly since the reservoir was charged with CO_2.

6.6 Stable Isotope Constraints on Fluid Origin and Sources of CO_2

Three populations are evident in the stable isotope data (Figure 8). The main calcite population (Calcite II and III) exhibits a relatively wide range of oxygen isotope values (0.2 to 5.1‰) and a narrower range of carbon isotope values (-7.5 to -5.2‰). Within this population, calcite cements from the gas-legs in Redman-1 and Ladbroke Grove-3 have low positive $\delta^{18}O$ values (<2.3‰), whereas calcite cements from the region of the GWC and water-leg at Ladbroke-3 have more positive $\delta^{18}O$ values (>3.6‰) (Figure 8). Calcite cements at Zema-1 lie at the boundary between the two subpopulations. The differences between samples from the gas-leg and water-leg in Redman-1 and Ladbroke Grove-3 cannot be due solely to the presence or absence of CO_2 currently within the reservoir since the gas column at Redman-1 is almost pure methane in contrast with moderately high CO_2 levels at Ladbroke Grove-3.

A second calcite population comprises a single calcite cement from the gas-leg of Ladbroke Grove-3 identified as Calcite I (2523.05m), which has a similar oxygen isotope composition to other calcites in the gas-leg but is strongly depleted in ^{13}C as are Calcite I^W samples from Ladbroke Grove-1 and other wells in the Otway Basin (Watson et al., 2004a, 2004b).

The third population comprises siderite cements from Ladbroke Grove-3 that have oxygen and carbon isotope compositions enriched in ^{13}C and ^{18}O relative to calcite from the same samples but overlap with Watson et al. (2004a) values for ferroan dolomite and ankerite in the Ladbroke Grove Field (Figure 8). These Fe-Mg carbonates (Siderite II) occur mainly in moderate and high CO_2 wells where they are seen to replace grain-coating chlorite and are in turn overprinted by pore-filling calcite (Calcite III). In the moderate CO_2 well (Ladbroke Grove-3), siderite/ankerite and late stage calcite occur together in three samples from the region of the GWC, which implies they precipitated from fluids that contained dissolved CO_2 sourced from the CO_2 reservoired in the Ladbroke Grove Field. One sample from the gas-leg of the reservoir at Ladbroke Grove-3 (2523.05m) also contains

minor siderite associated with partially dissolved calcite (Siderite II, Calcite I). It is likely this sample preserves an earlier generation of calcite in view of the very different carbon isotope composition of the calcite; it is not possible to draw any conclusions on the siderite as the conditions under which this siderite formed are poorly constrained.

6.6.1 Oxygen Source

In order to determine the fluid source, we used model temperatures of 80°C and 120°C and the oxygen isotope fractionation equations for calcite-water and siderite-water to calculate the oxygen isotope compositions of the fluid in equilibrium with calcite and siderite in the low CO_2 wells (Redman-1 and Zema-1) and the moderate CO_2 reservoir at Ladbroke Grove-3 (Table 9) (Carothers et al., 1988; O'Neil et al., 1969). Low temperature formation (<80°C) of the pore-filling calcite cements (Calcite II and III) is unlikely based on their paragenesis and the available formation temperature reports (Table 1). The calculated oxygen isotope compositions of fluids in equilibrium with the calcites are much lower than those reported for most mid- to low-latitude sedimentary basins (Clayton et al., 1966) and to those attained during burial diagenesis in many sedimentary basins (Clauer and Chaudhuri, 1995). This suggests meteoric dominated waters were involved in the precipitation of the calcite cements.

Calcite cements below 2561.0 m from the region of the GWC and the water-leg at Ladbroke Grove-3 have higher $\delta^{18}O$ values than calcite cements from the gas-leg of Ladbroke Grove-3 irrespective of paragenetic stage. These calcites likely precipitated between 80°C and 120°C, which results in calculated fluid oxygen isotope compositions from -18.6 to -12.8 ‰ and -15.8 to -10.0 ‰ for the carbonates above and below 2561.0 m core depth, respectively. The calculated fluid oxygen isotopic compositions for the gas-leg in Ladbroke Grove-3 (and Redman-1) are unusually low even for meteoric fluids that may reflect the isotopic composition of residual water within the gas-leg. It is possible that these calcites formed in the Late Mesozoic under somewhat higher temperature conditions resulting from high heat flow associated with rapid burial of the rift basin (cf. Duddy, 1997). However, this is considered unlikely in view of the paragenetic relationship between siderite II and calcite III in the vicinity of the GWC and the similar carbon isotope compositions of calcite II and III in the gas-leg and water-leg in Ladbroke Grove-3.

In an isothermal regime, carbonate mineralisation is a process that will lower the fluid oxygen isotope composition because carbonates are enriched in ^{18}O relative to the formation water from which they precipitate (e.g., Carothers et al., 1988; O'Neil et al., 1969). In water dominated systems, the effect of carbonate precipitation on the oxygen isotope composition of the fluid is rarely significant, whereas carbonate precipitation has the potential to significantly change the carbon

isotope composition of the fluid (cf. Zheng, 1990). We know relatively little, however, about the processes leading to carbonate precipitation in the gas-leg of reservoirs. Where CO_2 is present in the reservoir, this will dissolve into the formation water at the GWC but water will also dissolve into the CO_2 phase that has been shown experimentally to be quite reactive (Loring et al., 2011; Spycher et al., 2003). The anomalously low fluid oxygen isotopic compositions are recorded in gas-leg carbonates from both the low CO_2 well (Redman-1) and the moderate CO_2 well (Ladbroke Grove-3), which indicates they are not uniquely linked with relatively high levels of CO_2 in the reservoir. The occurrence of carbonates at Ladbroke Grove-3 close to the boundary between sandstones and finer grained lithologies is likely a response to facies-related differences in permeability, whereby the residual water is CO_2-saturated because gas is unable to migrate into the less permeable rocks. We know that ^{18}O will strongly partition from this water into any CO_2 in the gas phase (Bottinga, 1968) so perhaps even low levels of CO_2 in the gas-leg are sufficient to produce anomalously low $\delta^{18}O$ values in residual water and the carbonates that precipitate from this water. In this context, shifts in the $\delta^{18}O$ values of reservoir fluids after injection of CO_2 have been identified at several CO_2 storage sites and related to oxygen isotope exchange between CO_2 and water (Johnson et al., 2011; Kharaka et al., 2006). The proportion of CO_2 required to produce the observed shift of several per mil in the $\delta^{18}O$ value of water in the gas leg relative to water at and below the GWC at Ladbroke Grove-3 depends on the initial oxygen isotope composition of the water and CO_2; the latter is unknown and that precludes estimation of the fraction of CO_2 sourced oxygen in the system at the time of calcite precipitation (Johnson and Mayer, 2011; Johnson et al., 2011).

The difference between the oxygen isotope composition of siderite and calcite from the same sample (Table 9) mainly reflects the mineral-fluid fractionation factor as ^{18}O is partitioned more strongly into siderite than calcite (Carothers et al., 1988; O'Neil et al., 1969).

6.6.2 Carbon Source

The narrow range of $\delta^{13}C$ values (-7.5 to -5.2‰) for Calcite II and III across the low CO_2 wells (Redman-1 and Zema-1) and the moderate CO_2 well (Ladbroke Grove- 3), and their similarity with the $\delta^{13}C$ values of calcite and CO_2 in the high CO_2 Caroline Field (Watson et al., 2004a) may suggest that gas migrating into these reservoirs included a component of volcanic/mantle-derived CO_2. To test this hypothesis, we used model temperatures of 80°C and 120°C and the carbon isotope fractionation equations for calcite-water to calculate the carbon isotope compositions of the fluid in equilibrium with calcite in the study wells. Modelling of fluid carbon isotope composition is more complex than for oxygen isotopes as the mineral-fluid carbon isotope fractionation under aqueous conditions depends on the pH of the fluid. Under near neutral to acidic conditions (e.g., pH 6-7),

H_2CO_3 is the dominant aqueous carbonate species at temperatures less than 200°C, whereas HCO_3^- is the dominant species under near neutral to mildly alkaline conditions (e.g., pH >7; Large et al., 2001). The precipitation of calcite typically occurs under near neutral to alkaline conditions so the modelling of carbon isotope fractionation has been undertaken for the HCO_3^--dominant case using the fractionation equations of Ohmoto and Rye (1979) (Table 9). All samples of Calcite II and III have calculated carbon isotope fluid compositions at model temperatures of 80°C and 120°C in the range -8.8 to -6.5 ‰ that likely result from mixing between organic-derived ($\delta^{13}C$ value <-10 ‰) and magmatic/mantle ($\delta^{13}C$ value of ~-5 ‰) CO_2 (Hoefs, 1987). Notably, one calcite sample (Calcite I) from Ladbroke Grove-3 (2523.05m) is more depleted in ^{13}C, with a calculated carbon fluid composition less than -10 ‰ across the model temperature range that necessarily requires an organic carbon source (Table 9).

Modelling of fluid carbon isotope composition for the siderites has been undertaken for two end member scenarios (Table 9), one where H_2CO_3 is the dominant aqueous carbonate species (low pH fluid) and the other where HCO_3^- is the dominant aqueous carbonate species (higher pH fluid). We have used the calcite-fluid carbon isotope fractionation for siderite as there is no accurately determined siderite-fluid carbon isotope fractionation equation and the carbon isotope fractionation among carbonate phases is small at temperatures of 80 to 100°C (cf. Ohmoto and Goldhaber, 1997). Similar fluid carbon isotope values would be expected for the three siderite-calcite pairs from the region of the GWC at Ladbroke Grove-3 as these carbonates are all interpreted to have formed in equilibrium with the reservoired CO_2 in the field (Siderite II and Calcite III). A good match between the calculated siderite and calcite fluid compositions is obtained for the two samples below 2561.0 m (core depth) where the siderite formed under low pH conditions (Table 9). The siderite at 2561.0 m (Siderite I) appears to have formed under somewhat higher pH conditions.

6.7 Synthesis

Results from our study illustrate a complex diagenetic history for the Pretty Hill Formation with variations in the type and degree of reactions both between and within the four study wells. Many, but not all of these reactions are interpreted to be related to magmatic-sourced CO_2. Overall, paragenetic relationships observed from thin section and SEM are consistent between wells (low, moderate and high CO_2), although diagenetic reactions have progressed to different extents, which is partly a response to the reservoired CO_2-concentration and intra-reservoir heterogeneities.

The interpreted paragenetic sequence is generally consistent with those proposed in earlier work (e.g., Duddy, 1986; Little and Phillips, 1995; Watson et al., 2004a, 2004b). However, in this new study both petrographic observations and stable isotope data indicate that the majority of

carbonates (both calcite and siderite) are relatively late phases. Notably, dawsonite, which has often been suggested as a CO_2-capturing mineral phase (e.g., Hellevang et al., 2011, Worden, 2006), has not been observed in any of the samples. This research therefore provides evidence that the mineral dawsonite may not be a common product of natural rock-fluid-CO_2 gas interactions, and this needs to be considered when modelling CO_2-gas injection into sediments (cf. Xu et al., 2005).

In agreement with earlier work, an early generation of calcite is interpreted that predates CO_2-related diagenesis (Calcite I^W; Watson et al., 2004a) and locally overprints an early siderite generation (Siderite I^W); this calcite is depleted in ^{13}C and unrelated to the CO_2 in the Otway Basin. However, in contrast with previous work, there is no clear distinction in the carbon isotope compositions of most authigenic carbonates in the moderate CO_2 reservoir rocks and those in low CO_2 reservoir rocks in the study wells. These calcite and siderite samples have quite similar $\delta^{13}C$ values where differences between calcite and siderite in the same sample reflect mineral-fluid fractionation under somewhat different pH conditions. The calculated fluid carbon isotope compositions are similar to CO_2 in the Caroline Field where Chivas et al. (1987) have conclusively demonstrated a magmatic source for the CO_2. This may suggest that gas migration locally included magma-derived CO_2 that accumulated to varying degrees in the reservoirs and was the predominant carbon source for not only the Fe-Mg carbonates but also the sparry calcite cements in both the low and moderate CO_2 wells (Calcite II and III).

In summary, our results are consistent with previous observations suggesting that reaction of chlorite and feldspar is only likely to have occurred within sandstones where CO_2 has accumulated within the reservoir. These reactions are likely to be related to both facies and CO_2 concentration and require sufficient residence times and water saturations. The reactions are predicted to be most advanced at the changes between fluid phases (e.g., GWC), which might be associated with a structural spill point or related to grain size/facies variations within the gas leg (i.e. intraformational baffles). Lower feldspar content within the more permeable (high-CO_2) beds is interpreted to be a result of greater fluid-rock reaction, while lower CO_2 concentrations within less permeable beds has resulted in the preservation of much of the feldspathic component. Stable isotope data suggest that magma-derived CO_2 may have been more prevalent through the formation than previously thought, and that although the CO_2 is not currently present in the low CO_2 sites, it may have caused the local dissolution of carbonates and laumontite cement, and also contributed a source of carbon for late-stage calcite cements. Given that the low CO_2 sites show little other evidence of CO_2-related reaction, further work is recommended to study the carbonates in these low CO_2 sites and to see if the isotope results could be a result of low CO_2 residence time in the reservoir, and the lower

reactivity of both chlorite and feldspar relative to calcite and laumontite. Notably, Watson et al. (2004b) did not observe a significant degree of CO_2-related reaction in the Waarre Formation of the Caroline Field. However, given that the Caroline trap was probably filled in the past 5,000 years, and also that pre-production Sw were very low compared to high Sw at Garvoc-1 (Table 1), this lends support to the idea that both CO_2 reaction rates and water saturations may be major factors in the alteration of minerals and reservoir properties.

A revised paragenetic history for the Pretty Hill Formation is proposed below and illustrated on Figure 13.

All wells

1. Mechanical compaction, on-going through diagenesis
2. Early grain-coating chlorite, lithic chloritisation and minor siderite cementation (Siderite I) (alkaline pore fluids with high Fe concentrations)
3. Early calcite cementation (Calcite I) (alkaline pore fluids)
4. Feldspar albitisation and laumontite cementation (alkaline pore fluids)
5. Possible minor grain dissolution, laumontite dissolution, and associated kaolinite and quartz cementation (acidic pore fluids associated with decarboxylation of organic matter)
6. Liquid hydrocarbon migration with associated illitisation
7. Gas migration locally including magma-derived CO_2, ?laumontite dissolution, degradation/displacement of any liquid hydrocarbons and cementation by sparry calcite (Calcite II)

Moderate and high CO_2 wells

8. Calcite, chlorite and feldspar dissolution, and associated precipitation of kaolin, Fe-Mg carbonates (Siderite II), and authigenic quartz (acidic pore fluids related to magma-derived CO_2)
9. Late-stage calcite cementation (Calcite III) associated with reservoir heterogeneities and with carbon sourced from reservoired CO_2

6.8 Implications for Geological Storage of CO_2

The progress of fluid-flow and fluid-rock reactions in geological storage sites will depend on the flow of CO_2 in the reservoir, the dissolution of CO_2 into the formation brine, and the subsequent flow of CO_2-rich brines (Kampman et al., 2009). It is therefore logical to assume that differences in fluid-rock

reactions within a storage site will depend not only on the residence time of the CO_2, but also on the degree of heterogeneity/sandstone connectivity, and the flow properties of the reservoir rock.

Results from our study confirm this assumption. Data suggest that following CO_2 flux into a reservoir the dissolution of reactive minerals will proceed fastest within the most permeable lithologies. Calcite is generally considered to be one of the first minerals to dissolve. However, it is notable that early diagenetic calcite still occurs in some of our natural analogue samples, suggesting that dissolution rates of pre-existing carbonate cements will also be dependent on rock permeability and fluid chemistry.

Reactive clay minerals, such as chlorites, will react fairly rapidly and are likely to form kaolinite and siderite more-or-less *in situ*. Reaction of detrital feldspar is predicted to take a much longer time, but again, due to the low mobility of aluminium, will result in precipitation of kaolinite close to the dissolution sites. The almost complete reaction of feldspars at Garvoc-1 compared to Ladbroke Grove-3 could be evidence to suggest that the concentration of CO_2 may be a factor controlling the amount of feldspar reaction in the reservoir.

CO_2-induced reactions will occur at a much slower rate within the fine-grained interbeds of a storage interval due to the significantly smaller pores and lower permeability of these units, and thus higher capillary entry pressures. This is illustrated through the gas-leg of the Ladbroke Grove-3 well by the occurrence of relatively unaltered siltstone units (Fig. 9) and unaltered siltstone cuttings at the base reservoir/top seal contact; in both, kaolinite is a very minor component. Notably, however, siltstone cuttings in the very high CO_2 Garvoc-1 well are very kaolinitic, 5 m into the top seal (Fig. 12). Assuming that the kaolinite is a product of CO_2-reaction, the advanced alteration of minerals in fine-grained deposits at Garvoc-1 may be due to the much higher CO_2-content, a longer residence time, or a higher water saturation allowing transportation of ions. Jacob (1972) suggested that the effective permeability of the formation to CO_2 reduces rapidly with decreasing saturation of the CO_2, which could imply that with very high CO_2 concentrations there will be significant alteration of the siltstone beds within the storage interval. In contrast, preliminary observation from a natural analogue at Green River show mineral dissolution fronts have penetrated only tens of centimetres into the cored siltstone caprocks, suggesting that there would be little degradation by CO_2-charged fluids over a timeframe of hundreds of thousands of years (Kampman et al., 2009). Given this discussion, it is suggested here that the kaolinite-rich beds within the seal at Garvoc-1 might be more likely due to high water saturations and/or seal breach, which would have promoted flow of the CO_2-rich fluids (and earlier emplaced hydrocarbons) up-section.

The potential for carbonate cement precipitation as a mineral storage mechanism for injected CO_2 has been discussed in several publications (e.g., Watson et al., 2004a), and the results from this present work confirm the likelihood for minor- to moderate cementation by calcite, siderite or ankerite. Our results suggest that carbonates can occur throughout the reservoir interval, but are most likely to precipitate in significant amounts adjacent to fine-grained beds, including the top seal, and also close to the GWC, which we interpret to be due to differences in PCO_2 from high (in the reservoir due to high permeabilities) to relatively low (in baffles, seals, and below the CO_2-water contact). These observations suggest that fluid-mineral reactions help retard the diffusion distance of the CO_2 by forming carbonate cements, thereby increasing seal effectiveness. Heterogeneity of the reservoir interval would also be affected by increasing the potential for compartmentalisation and, depending on the time for precipitation, this may have an effect on injectivity or storage potential.

It is possible that quartz-kaolinite sandstones and kaolinitic siltstones as observed at Garvoc-1 may be the most likely outcome of CO_2 injection into a clastic storage site over geological time scales. This result, however, may be due to the very high water saturations at Garvoc-1 and as such may not be applicable to anthropogenic CO_2 storage sites; further natural analogue studies are recommended of very high CO_2 sites to provide some statistical validation of the data presented here. It is suggested that the mineralogical profile observed at Ladbroke Grove-3 might be more applicable to the relatively short-term effects of CO_2 storage (e.g., 1,000-5,000 year period). It is clear that both the mineralogy and the heterolithic nature of the deposits need to be understood, with any fine-grained horizons likely to act as baffles retarding both CO_2 flow and CO_2-reactions.

7. CONCLUSIONS

Reservoir facies from the Pretty Hill Formation are texturally similar in wells with low, moderate and high CO_2 levels. However, their detrital mineralogy is different, with lithic feldsarenites predominating in low and moderate CO_2 wells, and (diagenetically modified) sublitharenites occurring in the high CO_2 well. One explanation for this is that feldspar reactions have been extensive only in sandstones that were exposed to very high concentrations of CO_2 and associated with high water saturations.

The authigenic clay mineralogy in reservoir facies from wells with low CO_2 levels (including below the GWC at Ladbroke Grove-3) is dominated by chlorite, which is different to a dominant kaolinite composition within comparable facies from high CO_2 wells. Together with petrographic observations, this evidence suggests that under high PCO_2 conditions, chlorite undergoes almost

complete reaction to form kaolinite and other mineral products, thereby confirming the much faster reaction rate of chlorite relative to feldspars.

Evidence from our study suggests that reservoir heterogeneities locally present barriers to the flow of CO_2, which is demonstrated by vertical changes in the type and amount of mineral products. Where CO_2 is present in only moderate concentrations (i.e., Ladbroke Grove-3), fine-grained interbeds are kaolin-poor, which is interpreted to be largely due to impeded reactions. In contrast, where very high concentrations of CO_2 and high water saturations are present (i.e., Garvoc-1), the fine-grained interbeds are kaolin-rich, suggesting advanced CO_2-related reactions.

The distribution of carbonate cements also appears to be related to reservoir heterogeneities, with carbonate-rich zones concentrating near lithological boundaries. Results from our work imply that the greatest amount of CO_2-related reaction will occur at the basal CO_2-water contact and at reservoir-baffle/seal boundaries, which are effectively internal seals to the CO_2-charged fluids. Carbonate deposition has occurred close to these contacts at the reaction front, increasing the effectiveness of siltstones as seals, and hence increasing reservoir heterogeneity, which will have important long-term impacts on fluid-flow.

Contrary to previous studies, only one carbonate phase (Calcite I) has measured stable isotope values indicative of formation prior to both hydrocarbon and CO_2 emplacement; these cements are rare in the study wells. The more common carbonate phases (Calcite II, III, Siderite II) display significantly different $\delta^{13}C$ values to the early cement calcite phase, but with narrow ranges for each phase, regardless of whether the formation is within a low CO_2 or moderate CO_2 setting. Modelling has shown that these late-phase cements may have been derived from a component of volcanic/mantle derived CO_2, which is consistent with the similarity in stable isotope data between the late-phase cements and calcite/CO_2 currently reservoired in the high CO_2 Caroline Field. Given these results, together with the propensity for CO_2 migration and trap leakage into the structures of the Otway Basin, it is therefore suggested that CO_2 has migrated through the Pretty Hill Formation in some wells where CO_2 content is presently low.

The stable isotope results from carbonate cements at Redman-1 (low CO_2 well) are unexpected and inconsistent with the interpretations of Boult et al. (2004) who suggested that CO_2 is absent in the some gas fields of the central Penola Trough due to cross fault seal (Fig. 1). In addition, the abundance of chlorite at Redman-1 is a clear indication for limited CO_2, at least over any prolonged period. Evidence for Eocene volcanism has been given for some regions of the Penola Trough (e.g., Boult et al., 2008), which raises the possibility for migration of magma-derived CO_2 prior to the

Quaternary CO_2 accumulations. Further work is therefore recommended to investigate the origin of carbonate cements in this part of the Penola Trough in association with burial/temperature history, fluid/gas migration history, and pore water chemistry.

8. ACKNOWLEDGMENTS

The authors thank the CO2CRC for sponsoring this research and acknowledge the funding provided by the Commonwealth of Australia and industry sponsors through the CO2CRC Program. We thank the State of South Australia for providing Hylogger data, and CSIRO for providing The Spectral Assistant (TSA™) Viewer software. Analytical support was provided by Ben Durrant of GNS Science for thin section preparation, Liz Webber of Geoscience Australia for XRD analysis, Scott Brindle of Roberston for QEMSCAN analysis, and Kim Baublys for stable isotope analysis. We would also like to thank The Resources and Energy Group of the Department for Manufacturing, Innovation, Trade, Resources and Energy (DMITRE) for allowing core viewing and sampling, and Brad Field and Greg Browne (GNS Science) for their helpful comments on the manuscript.

9. REFERENCES

Alexander, E., 1992. Geology and petrophysics of petroleum reservoirs from the Otway Group, Otway Basin. Energy research and development corporation project no. 1424. Report Book 92/70. Department of Mines and Energy, South Australia.

Allen, J. L., Johnson, C. L., Heumann, M. J., Gooley, J., and Gallin, W., 2012. New technology and methodology for assessing sandstone composition: A preliminary case study using a quantitative electron microscope scanner (QEMScan): Geological Society of America Special Papers 2012, v. 487, p. 177-194.

Baines, S., and Worden R. H., 2004. The long term fate of CO_2 in the subsurface: natural analogues for CO_2 storage. In: S Baines and R H Worden eds. Geological Storage of Carbon Dioxide. Special Publication of the Geological Society, 59-85.

Baker, D., and Skinner, J., 1999. Well completion report, Redman-1, PEL 32 Otway Basin, South Australia. Open file envelope report no. 7539/6. Department of Primary Industries and Resources, South Australia.

Berman, M., Bischof, L., and Huntington, J.F., 1999. Algorithms and software for the automated identification of minerals using field spectra or hyperspectral imagery. Proc. of the 13th Int. Conf. on Applied Geologic Remote Sensing, Vancouver, Vol. 1, 222-232.

Bottinga, Y., 1968. Calculation of fractionation factors for carbon and oxygen isotopic exchange in the system calcite-carbon dioxide-water. Journal of Physical Chemistry, 72:800–808.

Boult, P.J., 1997. A review of seal potential in the Penola Trough, western Otway Basin (PEL32), Boral Energy Resources Ltd., internal report, unpublished.

Boult, P.J. and Hibburt, J.E. (eds.), 2002. The petroleum geology of South Australia, Volume 1: Otway Basin. Department of Primary Industries and Resources, South Australia.

Boult, P.J., Lyon, P.J., Camac, B., and McKirdy, D., 2004. Subsurface plumbing of the Penola Trough, Otway Basin. In: Boult, P.J., Johns, D.R., and Lang, S.C. (eds.), Eastern Australian Basins Symposium II, PESA, Special Publication, 483-498.

Boult, P., Lyon, P., Camac, B., Hunt, S., and Zwingmann, H., 2008. Unravelling the complex structural history of the Penola Trough – revealing the St George Fault. PESA Eastern Australasian Basins Symposium III, 81-94.

Burnham, A.K., and Sweeney, J.J., 1989. A chemical kinetic model of vitrinite maturation and reflectance. Geochimica et Cosmochimica Acta, 53, 2649-2657.

Burns, B.J., 1992. Isotopic analysis of gas from Boggy Creek-1 well Otway Basin. Report for Johnstone Environmental Technology. JET0165-02, unpublished.

Carothers, W.W., Lanford, H.A., and Rosenbauer, R.J., 1988. Experimental oxygen isotope fractionation between siderite-water and phosphoric acid liberated CO_2-siderite. Geochimica et Cosmochimica Acta, 52:2445-2450.

Chatfield, K., 1992. The relationship between volcanics, associated intrusives and carbon dioxide within the Otway Basin, South Australia. University of Adelaide. BSc (Hons) thesis (unpublished).

Chivas, A.R., Barnes, I., Evans, W.C., Lupton, J.E., and Stone, J.O., 1987. Liquid carbon dioxide of magmatic origin and its role in volcanic eruptions. Nature 326, 587-589.

Clauer, N., and Chaudhuri, S., 1995. Clays in Crustal Environments: Isotope Dating and Tracing. Springer Verlag, Heidelberg, Berlin, New York, 359 pp.

Clayton, R.N., Friedman, I., Graf D.L., Mayeda, T.K., Meents, W.F., and Shimp N.F., 1966. The origin of saline formation waters. Journal of Geophysical Research - Solid Earth, 71:3869-3882.

Cockshell, C.D., O'Brien, G.W., McGee, A., Lovibond, R., Perincek, D., and Higgins, R., 1995. Western Otway Basin Crayfish Group troughs. The APPEA Journal 35, 385-403.

Cudahy, T.J., Hewson, R., Caccetta, M., Roache, A., Whitbourn, L., Connor, P., Coward, D., Mason, M., Yang, K., Huntington, J., and Quigley, M., 2009. Drill core logging of plagioclase feldspar composition and other minerals associated with Archaean gold mineralisation at Kambalda Western Australia, using a bi-directional thermal infrared reflectance system. Reviews in Economic Geology v. 16, 223-235.

Duddy, I.R., 1986. Mineralogical and absolute chemical changes during burial of volcanogenic sediments. In: Sediments Down Under. 12th International Sedimentological Congress. Canberra, Australia. Abstracts, 87pp.

Duddy, I.R., 1997. Focussing exploration in the Otway Basin: Understanding timing of the source rock maturation. APPEA Journal 37, 178-191.

Folk, R.L., Andrews, P.B. and Lewis, D.W., 1970. Detrital sedimentary rock classification and nomenclature for use in New Zealand. New Zealand Journal of Geology and Geophysics 13, 937-968.

Gaus, I., 2009. Role and impact of CO_2-rock interactions during CO_2 storage in sedimentary rocks. International Journal of Greenhouse Gas Contr. 4, 73-89.

Geological Survey of Victoria, 1995. The stratigraphy, structure, geophysics and hydrocarbon potential of the Eastern Otway Basin. Geological Survey of Victoria Report 103.

Gherardi, F., Xu, T.F., and Pruess, K., 2007. Numerical modeling of self-limiting and self-enhancing caprock alteration induced by CO_2 storage in a depleted gas reservoir. Chemical Geolology 244, 103.

Golding, S., Uysal, T., Bolhar, R., Boreham, C., Dawson, G., Baublys, K., and Esterle, J., 2013. Carbon dioxide-rich coals of the Oaky Creek area, central Bowen Basin: a natural analogue for carbon sequestration in coal systems. Australian Journal of Earth Sciences, 60:125-140.

Gottlieb, P., Wilkie, G., Sutherland, D., Ho-Tun, E., Suthers, S., Perera, K., Jenkins, B., Spencer, S., Butcher, A., and Rayner, J., 2000. Using quantitative electron microscopy for process mineralogy applications. Journal of the Minerals, metals and Materials Society, 52, 24-25.

Gravestock, D.I., Hill, A.J., and Morton, J.G.G., 1986. A review on the structure, geology and hydrocarbon potential of the Otway Basin in South Australia. Department of Mines and Energy SA (unpublished report 86/77).

Haszeldine, R.S., Quinn, O., England, G., Wilkinson, M., Shipton, Z.K., Evans, J.P., Heath, J., Crossey, L., Ballentine, C.J., and Graham, C.M., 2005. Natural geochemical analogues for carbon dioxide storage in deep geological porous reservoirs, a United Kingdom perspective. Oil and Gas Science and Technology – Rev. IFP 60, 33-49.

Hellevang, H., Aagaard, P., Oelkers, E.H., and Kvamme, B., 2005. Thermodynamic and kinetic stability of dawsonite ($NaAl(OH)_2CO_3$) – will it act as a storage host during CO_2 capture? Geophysical Research Abstracts, 7.

Hellevang, H., Declercq, J., and Aagaard, P., 2011. Why is dawsonite absent in CO_2 charged reservoirs? Oil & Gas Science and Technology - Revue de l'IFP 66 (1), 119–135.

Higgs, K., 2011. A review of onshore Australian basins as natural analogues for geological storage. Cooperative Research Centre for Greenhouse Gas Technologies, Canberra, Australia, CO2CRC Publication Number RPT11-2810. 36pp.

Higgs, K., Funnell, R., and Reyes, A., 2012. Changes in reservoir heterogeneity and quality as a response to high partial pressures of CO_2 in a gas reservoir, New Zealand. Jounal of Marine and Petroleum Geology, 32, 110-137.

Hoefs, J., 1987. Stable Isotope Geochemistry. Springer-Verlag, Berlin, 241 pp.

Huntington, J., Whitbourn, L., Mason, P., Berman, M., and Schodlok, M.C., 2010. HyLogging – voluminous industrial-scale reflectance spectroscopy of the earth's subsurface. Art, Science and Applications of Reflectance Spectroscopy Symposium, Boulder, CO, 14 pp.

Jacob, B., 1972. Dynamics of Fluids in Porous Media (New York).

Johnson, G. and Mayer, B., 2011. Oxygen isotope exchange between H_2O and CO_2 at elevated CO_2 pressures: Implications for monitoring of geological CO_2 storage. Applied Geochemistry 26, 1184-1191.

Johnson, G., Mayer, B., Nightingale, M., Shevalier, M., and Hutcheon, I., 2011. Using oxygen isotope ratios to quantitatively assess trapping mechanisms during CO_2 injection into geological reservoirs: The Pembina case study. Chemical Geology 283, 185-193.

Jones, R.M., Boult, P., Hillis, R.R., Mildren, S.D., and Kaldi, J., 2000. Integrated hydrocarbon seal evaluation in the Penola Trough, Otway Basin. APPEA Journal 40, 194-211.

Kampman, N., Bickle, M., Becker, J., Assayag, N., and Chapman, H., 2009. Feldspar dissolution kinetics and Gibbs free energy dependence in a CO_2-enriched groundwater system, Green River, Utah. Earth and Planetary Science Letters 284, 473-488.

Kampman, N., Maskell, A., Bickle, M.J., Evans, J.P., Schaller, M., Purser, G., Zhou, Z., Gattacceca, J., Peitre, E.S., Rochelle, C.A., Ballentine, C.J., and Busch, A., 2013. Scientific drilling and downhole fluid sampling of a natural CO_2 reservoir, Green River, Utah. Scientific Drilling 16, 33-43.

Kharaka, Y.K., Cole, D.R., Hovorka, S.D., Gunter, W.D., Knauss, K.G. and Freifield, B.M., 2006. Gas-water-rock interactions in Frio Formation following CO2 injection: implications for the storage of greenhouse gases in sedimentary basins. Geology 34, 577-580.

Kirste, D.M., Watson, M.N., and Tingate, P.R., 2004. Geochemical modelling of CO_2-water-rock interaction in the Pretty Hill Formation, Otway Basin. PESA Eastern Australian Basins Symposium II, 403-411.

Kopsen, E., and Scholefield, T., 1990. Prospectivity of the Otway Supergroup in the central and western Otway Basin. APPEA Journal 30, 263-279.

Large, R.R., Bull, S.W., and Winefield, P.R., 2001. Carbon and oxygen isotope halo in carbonates related to the McArthur River (HYC) Zn-Pb-Ag deposit, north Australia: implications for sedimentation, ore genesis and mineral exploration. Economic Geology, 96:1567-1593.

Leslie, R.B., and Sell, B.H., 1968. Interstate/Shell Garvoc No. 1 well, Otway Basin, Victoria, well completion report. Report no. PE902876. Department of Natural Resources and Environment, Victoria, Australia.

Little, B.M., 1996. The petrology and petrophysics of the Pretty Hill Formation in the Penola Trough, Otway Basin. University of South Australia MSc thesis, unpublished.

Little, B.M., and Phillips, S.E., 1995. Detital and authigenic mineralogy of the Pretty Hill Formation in the Penola Trough, Otway Basin: Implications for future exploration and production. APPEA Journal 35, 538-571.

Loring, J.S., Thompson, C.J., Wang, Z., Joly, A.G., Sklarew, D.S., Schaef, H.T., Ilton, E.S., Rosso, K.M., and Felmy, A.R., 2011. In situ infrared spectroscopic study of forsterite carbonation in wet supercritical CO_2. Environmental Science & Technology, 45: 6204-6210.

Lovibond, R., Suttill, R.J., Skinner, J.E. and Aburas, A.N., 1995. The hydrocarbon potential of the Penola Trough, Otway Basin, APPEA Journal 35, 358-371.

Lyon, P.J., Boult, P.J., Watson, M., and Hillis, R.R., 2005. A systematic fault seal evaluation of the Ladbroke Grove and Pyrus traps of the Penola Trough, Otway Basin. APPEA Journal 45, 459-476.

Martin, K.R., and Baker, J.C., 1993. Petrology, diagenesis and reservoir quality of the Pretty Hill Sandstone, Otway Basin, South Australia. Department of Mines and Energy, South Australia.

McCrea, J. M., 1950. On the isotopic chemistry of carbonates and a paleotemperature scale. Journal of Chemical Physics, 18, 49-857.

McDougall I., Allsopp, H.L., and Chamalaun, F.H., 1966. Isotopic dating of the Newer Volcanics of Victoria, Australia, and geomagnetic polarity epochs. Journal of Geophysical Research 71, 107-117.

Moore, J., Adams, M., Allis, R., Lutz, S., and Rauzi, S., 2005. Mineralogical and geochemical consequences of the long-term presence of CO_2 in natural reservoirs: An example from the Springerville–St. Johns Field, Arizona, and New Mexico, U.S.A. Chemical Geology 217, 365-385.

Morton, J.G.G., 1990. Revisions to stratigraphic nomenclature of the Otway Basin, South Australia. Quarterly Geological Notes No 116, Geological Survey of South Australia.

Mulready, J., 1977. The Caroline carbon dioxide field and associated carbon dioxide occurrences, Gambier Embayment, South Australia. The APPEA Journal 17, 121-127.

Ohmoto, H., and Goldhaber, M.B., 1997. Sulfur and carbon isotopes, In: Barnes, H.L. (ed.), Geochemistry of Hydrothermal Ore deposits - third edition. New York, Wiley, p. 517-612.

Ohmoto, H., and Rye, R.O., 1979. Isotopes of sulfur and carbon. In: Barnes, H.L. (ed.), Geochemistry of Hydrothermal Ore Deposits - second edition. New York, Wiley, p. 509-567.

O'Neil, J.R., Clayton, R.N., and Mayeda, T.K., 1969. Oxygen isotope fractionation in divalent metal carbonates. Journal of Chemical Physics, 51:5547-5548.

Padley, D., McKirdy, D.M., Skinner, J.E., Summons, R.E., and Morgan, R.P., 1995. Crayfish Grouphydrocarbons — implications for palaeoenvironment of Early Cretaceous rift fill in the western OtwayBasin. APPEA Journal, 35, 517-537.

Parker, K.A., 1992. The exploration and appraisal history of the Katnook and Ladbroke Grove gas fields, onshore Otway Basin, South Australia. The APPEA Journal 32, 67-85.

Parker, G.J., 1995. Early Cretaceous stratigraphy along the northern margin of the Otway Basin, Victoria. Victorian Initiative for Minerals and Petroleum Report 23. Department of Agriculture, Energy & Minerals.

Pearce, J., Holloway, S., Wacker, H., Nelis, M., Rochelle, C., and Bateman, K., 1996. Natural occurrences as analogues for the geological disposal of carbon dioxide. Energy Conversion and Management, 37, p. 1123-1128.

Perincek, D., and Cockshell, C.D., 1995. The Otway Basin: Early Cretaceous rifting to Neogene inversion. APPEA Journal 35, 451-466.

Phillips, S.E., 1991. Petrology report, Katnook 3, Otway Basin. Amdel Core Services report. South Australia. Department of Primary Industries and Resources. Open file Envelope report no. 7250(2). Department of Primary Industries and Resources, South Australia.

Pirrie, D., Butcher, A. R., Power, M. R., Gottlieb, P., and Miller, G. L., 2004. Rapid quantitative mineral and phase analysis using automated scanning electron microscopy (QemSCAN): Potential application in forensic geosciences, in Pye, K., and Crodt, D. J., eds., Forensic Geoscience: Principles, Techniques and Applications: Geological Society [London] Special Publication v. 232, p. 123–136.

Sagasco Resources Ltd., 1992. Zema-1 well completion report, PEL 32, Otway Basin, South Australia. Open File Envelope report no. 7410/6. Department of Primary Industries and Resources, South Australia.

Sheard, M., 1995. Quaternary volcanic activity and geological hazards. In: Drexel, J.F. and Preiss, W.V. (ed.), The Geology of South Australia, 2, The Phanerozoic GSSA, Bulletin, 54, 264-268.

Simeone, S.F., and Mitchell, J.A., 2001. Ladbroke Grove-3 well completion report. PPL-62 South Australia Report for Origin Energy Resources Limited. Department of Primary Industries and Resources, South Australia.

Spycher, N., Pruess, K., and Ennis-King, J., 2003. CO_2-H_2O mixtures in the geological sequestration of CO_2. I. Assessment and calculation of mutual solubilities from 12 to 100°C and up to 600 bar. Geochimica et Cosmochimica Acta, 67: 3015-3031.

Stevens, S H., Pearce, J.M., and Rigg, A.A.J., 2003. Natural analogues for geologic storage of CO_2: an integrated global research program. In: First national conference on carbon sequestration, US Department of Energy, National Energy Technology Laboratory, May 2001.

Surdam, R.C., Boese, S.W., and Crossey, L.J., 1984. The chemistry of secondary porosity. In: Surdam, R.C., McDonald, D.A., (Eds.), Clastic Diagenesis, American Association of Petroleum Geologists, Memoir 37, 127-150.

Uysal, I.T., Golding, S.D., Bolhar, R., Zhao, J.X., Feng, Y.X., Baublys, K.A., and Greig, A., 2011. CO_2 degassing and trapping during hydrothermal cycles related to Gondwana rifting in eastern Australia. Geochimica et Cosmochimica Acta, 75:5444-5466.

Von Der Borch, C.C., Conolly, J.R., and Dietz, R.S., 1970. Sedimentation and structure of the continental margin in the vicinity of the Otway Basin, Southern Australia. Marine Geology 8, 59-83.

Watson, M, 2012. Natural CO_2 Accumulations as Analogues for CO_2 Geological Storage and CO_2-Induced Diagenesis in the Otway Basin, Australia. PhD Thesis.

Watson, M.N., Boreham, C.J., and Tingate, P.R., 2004a. Carbon dioxide and carbonate cements in the Otway Basin: implications for geological storage of carbon dioxide. APPEA Journal 44, 703-720.

Watson, M.N., Zwingmann, N., and Lemon N.M., 2004b. The Ladbroke Grove-Katnook carbon dioxide natural laboratory: a recent CO_2 accumulation in a lithic sandstone reservoir. Energy, Vol. 29 (9-10), p. 1457 – 1466.

Watson, M.N., Zwingmann, N, Lemon, N.M., and Tingate, P.R., 2003. Onshore Otway Basin carbon dioxide accumulations: CO_2-induced diagenesis in natural analogues for underground storage of greenhouse gas. APPEA Journal 43, 637-653.

Wilkinson, M., Haszeldine, S., Fallick, A.E., Olding, N., Stoker, S., and Gatliff, R.W, 2009. CO_2-mineral reaction in a natural analogue for CO_2 storage – implications for modelling. Journal of Sedimentary Research, 79, 486-494.

Worden, R.H., 2006. Dawsonite cement in the Triassic Lam Formation, Shabwa Basin, Yemen: A natural analogue for a potential mineral product of subsurface CO_2 storage for greenhouse gas reduction. Marine and Petroleum Geology 23, 61-77.

Xu, T., Apps, J.A., and Pruess, K., 2005. Mineral sequestration of carbon dioxide in a sandstone-shale system. Chemical Geology 217, 295-318.

Zheng, Y.F., 1990. Carbon-oxygen isotopic covariation in hydrothermal calcite during degassing of CO_2 - A quantitative evaluation and application to the Kushikino gold mining district in Japan. Mineralium Deposita, 25:246-250.

Well	Redman-1	Zema-1	Ladbroke Grove-3	Garvoc-1
Well Location	Penola Trough	Penola Trough	Penola Trough	Port Campbell Embayment
Spud Date	1998	1992	1999	1968
Structure	Tilted fault block	Tilted fault block	Anticline with fault-bounded closure to the north	Gravity nose within the N Hinge Zone
Inclination	Slt deviation	Near vertical	Deviated	Near vertical
Top Pretty Hill Fm	2810 m	2403.2 m	2503 m	1362.5 m (4470 ft)
Total Depth	2957 m	2733.5 m	2693.7 m	1535 m (5035 ft)
Hydrocarbons	74 m gas column; perched residual oil recovered from core plugs	Good gas and poor fluorescence from 2400 m to 2730 m	64.3 m gas column	Gas shows; traces of oil in the cores
Conventional Cores	2828.8-2846.8 m	1) 2412-2430.3 m 2) 2430.3-2448.3 m 3) 2448.3-2466.3 m	1) 2502-2520 m 2) 2520-2547.2 m 3) 2547.2-2575 m	1379.5-1385.6 m (4526-4546 ft)
Core Shift	+ 3.8 m	+3.6 m	+3.5 m	None applied
DST	2827.5-2857.5 m	2399-2415 m	No	1365-1386 m (4478-4548 ft)
DST result	Gas composed of almost pure methane	Gas flow to surface at a rate too small to measure	N/A	Water cut with CO_2
CO_2 Content of Gas	Low (<0.1 mol%)	Low (<0.3 mol%)	Moderate 29.2-56.6%, with decreasing CO_2 content uphole	High (96.7 mol%)
Production Test	Yes	No	Yes	No
RFT / MDT	Yes	Yes	Yes	No
RFT / MDT sample	2876 m (gas) 2899 m (water)	2427.7 m (water/filtrate)	2515-2567.9 m (gas)	N/A
Free Water Level (FWL)	2884.5 m	N/A	2567.3 m	N/A
Reservoir Water Saturation	48%	92.6-100%	26-89%	78-100%
Reservoir Temperature	116 °C	105 °C	108 °C	75 °C
Hydrocarbon Fluid Properties	52 °API	N/A	38 °API	N/A
Hydrocarbon Source	lower Crayfish Group	N/A	Crayfish Group	N/A
Result	Gas/condensate production	Plugged and abandoned with an 86 m paleo-gas leg and a 15 m paleo-oil leg	Gas/condensate production	Plugged and abandoned

Table 1. Study well information. Data from Baker and Skinner (1999), Boult and Hibburt (2002), Jones et al. (2000), Leslie and Sell (1968), Sagasco Resources Ltd. (1992), Simeone and Mitchell (2001). All depths m MDKB (measured depth below Kelly bushing).

Wavelength Region	Wavelength Range (nm)	Mineralogy
VNIR	400 - 1100	Iron oxides and hydroxides manganese oxides, rare earths
SWIR	1100 - 2500	Hydroxyls (aluminium, manganese and iron), carbonates, sulphates, micas. amphiboles
TIR	5000 - 14000	Carbonates, silicates, including quartz, feldspar, plagioclase, olivine, pyroxene, garnet

Table 2. Common minerals detected at different wavelengths using Hylogger^{TM} version 3 and TSG^{TM} software.

Well	Sample Depth (m)	Sample Depth (ft)	Gradient	Sample Type	Thin Section	SEM	QEMSCAN	XRD	Isotopes
	2827.53		Gas	Core				✓	
	2832.10		Gas	Core	✓	✓			✓
Redman-1	2832.98		Gas	Core	✓	✓			
	2833.15		Gas	Core	✓	✓		✓	
	2841.65		Gas	Core	✓	✓		✓	
	2418.61		Water	Core	✓	✓			✓
	2426.75		Water	Core	✓	✓		✓	
	2426.95		Water	Core	✓	✓		✓	
	2447.06		Water	Core	✓	✓	✓	✓	
Zema-1	2453.56		Water	Core	✓	✓	✓		✓
	2459.65		Water	Core	✓	✓		✓	
	2459.95		Water	Core	✓	✓	✓	✓	
	2465.75		Water	Core	✓	✓		✓	
	2499		Gas	Cuttings			✓		
	2502		Gas	Cuttings			✓		
	2505		Gas	Cuttings			✓		
	2506.81		Gas	Core	✓	✓			✓
	2508		Gas	Cuttings			✓		
	2508.50		Gas	Core	✓	✓		✓	
	2508.65		Gas	Core	✓	✓		✓	
	2523.05		Gas	Core	✓	✓		✓	✓
	2523.90		Gas	Core				✓	
Ladbroke	2524.90		Gas	Core				✓	
Grove-3	2557.30		Gas	Core	✓	✓		✓	✓
	2561.00		Gas	Core	✓	✓	✓	✓	✓
	2565.67		Transition	Core	✓	✓	✓		✓
	2566.25		Transition	Core	✓*				
	2566.30		Transition	Core	✓*				
	2566.58		Transition	Core	✓	✓	✓		✓
	2568.63		Water	Core	✓*		✓		
	2570.85		Water	Core	✓	✓	✓		✓
	2572.54		Water	Core	✓*				
	2572.88		Water	Core	✓	✓		✓	✓
	1359.41	4460	CO_2/Water	Cuttings			✓		
	1362.46	4470	CO_2/Water	Cuttings			✓		
	1365.50	4480	CO_2/Water	Cuttings			✓		
	1368.55	4490	CO_2/Water	Cuttings			✓		
	1371.60	4500	CO_2/Water	Cuttings			✓		
	1374.65	4510	CO_2/Water	Cuttings			✓		
	1386.84	4550	CO_2/Water	Cuttings			✓		
	1379.85		CO_2/Water	Core	✓	✓	✓		
	1380.35		CO_2/Water	Core	✓	✓	✓		
	1381.08		CO_2/Water	Core	✓	✓			
Garvoc-1	1380.83		CO_2/Water	Core	✓	✓			
	1381.63		CO_2/Water	Core	✓	✓	✓		
	1382.49		CO_2/Water	Core	✓	✓			
	1382.95		CO_2/Water	Core	✓	✓	✓		
	1383.18		CO_2/Water	Core	✓	✓			
	1478.28	4850	Water	Cuttings			✓		
	1490.47	4890	Water	Cuttings			✓		
	1496.57	4910	Water	Cuttings			✓		
	1505.71	4940	Water	Cuttings			✓		
	1514.86	4970	Water	Cuttings			✓		

Table 3. Sample and analysis list. * represents qualitative petrographic analysis.

Well	Sample Depth (m)	CO_2	Gradient	Mean Grain Size				Max Grain Size		Sorting	
				mm	micron	phi	Class	mm	Class	St Dev	Class
Redman-1	2832.09	Low	Gas	0.26	265	1.917	mL	2.23	granule	0.5964	Moderately good
	2832.98	Low	Gas	0.15	153	2.705	fL	0.36	mU	0.6116	Moderately good
	2833.15	Low	Gas	0.19	187	2.420	fU	0.53	cL	0.6079	Moderately good
	2841.65	Low	Gas	0.33	330	1.600	mL	0.94	cU	0.7363	Moderate
Zema-1	2418.61	Low	Water, gas shows	0.41	407	1.295	mU	0.99	cU	0.6558	Moderately good
	2426.75	Low	Water, gas shows	0.45	454	1.140	mU	1.38	vcL	0.6675	Moderately good
	2426.95	Low	Water, gas shows	0.36	363	1.462	mU	0.73	cU	0.5782	Moderately good
	2447.06	Low	Water, gas shows	0.21	209	2.259	fU	0.42	mU	0.4078	Good
	2453.56	Low	Water, gas shows	0.19	188	2.413	fU	0.37	mU	0.4789	Good
	2459.65	Low	Water, gas shows	0.15	151	2.725	fL	0.28	mL	0.5009	Moderately good
	2459.95	Low	Water, gas shows	0.19	193	2.373	fU	1.18	vcL	0.7241	Moderate
	2465.75	Low	Water, gas shows	0.22	220	2.182	fU	0.55	cL	0.6193	Moderately good
Ladbroke Grove-3	2506.81	Moderate	Gas	0.14	139	2.849	fL	0.31	mL	0.5348	Moderately good
	2508.50	Moderate	Gas	0.12	117	3.098	vfU	0.24	fU	0.5351	Moderately good
	2508.65	Moderate	Gas	0.13	128	2.968	fL	0.27	mL	0.5634	Moderately good
	2523.05	Moderate	Gas	0.38	383	1.383	mU	1.54	vcU	0.6446	Moderately good
	2557.30	Moderate	Gas	0.14	137	2.868	fL	0.26	mL	0.4830	Good
	2561.00	Moderate	Gas	0.31	312	1.679	mL	0.60	cL	0.6409	Moderately good
	2565.67	Moderate	Transition	0.59	585	0.773	cL	2.45	granule	0.6148	Moderately good
	2566.58	Low (below GWC)	Transition	0.20	197	2.343	fU	0.36	mU	0.5077	Moderately good
	2570.85	Low (below GWC)	Water	0.24	239	2.068	fU	0.52	cL	0.5670	Moderately good
	2572.88	Low (below GWC)	Water	0.29	292	1.776	mL	3.00	granule	0.8657	Moderately poor
Garvoc-1	1379.85	High	Water, gas shows	0.44	438	1.193	mU	2.25	granule	1.0412	Poor
	1380.35	High	Water, gas shows	0.43	426	1.231	mU	0.94	cU	0.7082	Moderately good
	1380.83	High	Water, gas shows	0.46	457	1.131	mU	1.40	vcL	0.8209	Moderate
	1381.08	High	Water, gas shows	0.37	369	1.437	mU	1.23	vcL	0.6695	Moderately good
	1381.63	High	Water, gas shows	0.33	328	1.609	mL	0.82	cU	0.7114	Moderate
	1382.49	High	Water, gas shows	0.36	356	1.490	mU	0.85	cU	0.6443	Moderately good
	1382.95	High	Water, gas shows	0.33	333	1.586	mL	1.15	vcL	0.7250	Moderate
	1383.18	High	Water, gas shows	0.40	400	1.321	mU	0.93	cU	0.6966	Moderately good

Table 4. Summary of grain size and sorting characteristics from point-count data (core samples).

Table 5. Summary of mineralogy and visible porosity from point-count data (core samples; data presented as volume %; Tr = trace; zero values are left blank). Under dominant carbonate phase, CI = early calcite, CII & CIII = late pore-filling calcite, SI = early siderite, SII = late grain-coating siderite, (a) = sample with stable isotopic analysis of single phase, (a*) = sample with stable isotopic analysis of grain-coating siderite and pore-filling calcite phases.

					GRAINS (%)							AUTHIGENIC CLAYS (%)					OTHER AUTHIGENIC CEMENTS (%)								
Well	**Sample Depth (m)**	**Macroporosity (%)**	**Detrital Matrix (%)**	**Residual Hydrocarbons (%)**	**Total Grains**	Quartz	Feldspar	Lithic Fragments	Degraded Grains (lithics/feldspar)	Mica	Other Grains	**Total Authigenic Clay**	Chlorite and Chlorite/Smectite	Kaolinite/Dickite	Illite and Illitised Kaolinite	Other Mixed Layer Clay	**Total Other Cement**	Quartz Overgrowths	Feldspar	Laumonite	Calcite	Dolomite	Siderite/Ankerite	Opaques	**Dominant Carbonate Phase**
Redman-1	2832.09	0.7			71.3	24.3	23.6	13.7	4.7	2.4	2.6	4.7				4.7	23.2	1	0.3		20.7		Tr	1.2	CII (a)
	2832.98	0.3			78.5	16.4	26.7	29.1	3.7	2	0.6	18.6	17.3	0.3		1.0	2.6		Tr		0.6		Tr	2.0	CII
	2833.15		1.0		70.8	16.7	30.3	17.2	4.3	2	0.3	23.0	22.0			1.0	5.0	0.7	Tr		2.0		Tr	2.3	CII
	2841.65	3.7		14.0	70.9	42.6	14.3	12.3	0.7	1		9.7	7.7			2.0	1.6	0.3			1.0		0.3		CII
Zema-1	2418.61	1.3	0.3		68.1	46.3	10.3	8.6	0.3	0.3	2.3	15.3	15.3				14.7	1.0			11.7			2.0	CIII (a)
	2426.75	10.6			65.4	47.4	8	8	1.3		0.7	22.4	21.7			0.7	1.6	0.3			1.0		Tr	0.3	CIII
	2426.95	13.4		0.3	62.2	37.7	10	11.2	0.3		3	22.0	21.7			0.3	2.1	0.7			1.4				CIII
	2447.06	0.3			74.1	23.4	25.7	20.4	3.3	0.3	1	23.3	20.7		0.3	2.3	2.2	0.3	Tr		0.3		Tr	1.6	
	2453.56		0.7		72.0	11.7	27	26.9	4.7	1.7		4.7	2.0			2.7	22.6		Tr		20.3		0.3	2.0	CII (a)
	2459.65				70.2	11.9	29.6	20.4	5.3	2.7	0.3	10.0	7.7		0.3	2.0	19.6				17.3		Tr	2.3	CII
	2459.95	0.3			73.0	16.4	31.6	20.4	2.3	2	0.3	24.3	23.6			0.7	2.6	0.3	Tr	0.3			Tr	2.0	
	2465.75				67.4	18.3	26	18	3.7	0.7	0.7	26.2	25.3	0.3	0.3	0.3	6.3	2.7	1.3	1.3	0.3		Tr	0.7	
Ladbroke Grove-3	2506.81				72.3	19.0	30.4	15.3	6.3	0.3	1	5.4				5.4	22.3				19.0		0.7	2.6	CII (a)
	2508.50	5.0		0.7	65.6	18.3	25.6	12.3	5	3.4	1	9.3	0.6	3.3		5.4	19.3	0.7			1.3		13.7	3.6	SII
	2508.65	5.3	0.3	0.7	70.0	14.0	32.3	16.7	5.3	1.7		14.7	4.7	4.0		6.0	9.0	4.7			0.3		2.0	2.0	SII
	2523.05			0.6	66.3	33.3	19	10.4	2.3	1	0.3	11.7	0.7	2.6	1.0	7.4	21.3	1.0			14.0	0.3	3.0	3.0	CI (a*)
	2557.30		0.3		59.1	17.9	23	13.6	3.3	0.6	0.7	5.3		0.3		5.0	35.0				31.0		0.7	3.3	CII (a)
	2561.00	0.3			71.3	35.7	23	10.6	1.7	0.3		15.9	0.3	12.0	0.3	3.3	12.2	4.0			0.3	0.3	5.3	2.3	SII (a*)
	2565.67				71.3	49.3	13	7.4	1.3		0.3	14.3		10.0		4.3	14.4	0.7			4.4		8.3	1.0	SII/CIII (a*)
	2566.58		0.3		67.5	19.0	27.7	17.1	2.7	0.7	0.3	14.3	5.6	0.7	0.3	7.7	17.9	0.7			7.6	0.3	9.0	0.3	SII/CIII (a*)
	2570.85	0.3			74.7	22.3	28.7	20	2.7	0.7	0.3	19.8	15.4	1.0	1.0	2.4	5.3				3.7			1.6	?CII (a)
	2572.88	0.3	1.7		63.9	24.0	25	10.3	2.3	1.3	1	25.6	21.7		2.3	1.6	8.4	0.7			1.0		0.3	6.4	?CII (a)
Garvoc-1	1379.85	0.3	9.0		63.6	53.7	0.3	5	3.3	0.3	1	15.9	2.9	5.7	0.3	7.0	11.0	2.3					0.3	8.4	SII
	1380.35	6.0	0.7	0.3	53.7	48.7	1	2.6	0.7		0.7	28.6	0.3	22.7	1.0	4.6	10.6	3.3				0.3	4.7	2.3	SII
	1380.83	2.2	0.7		61.0	53.3	1	5.7	1			28.9		24.7	0.3	3.9	7.0	3.3					2.3	1.4	SII

1381.08	3.6	1.0	55.6	48.0	0.7	5.3	1.3		0.3	30.9	0.7	22.9	1.0	6.3	8.6	3.0			2.3	3.3	SII
1381.63	2.3	2.0	53.4	46.0	0.7	5	1	0.7		31.9	0.3	26.0	0.9	4.7	10.4	4.0			3.7	2.7	SII
1382.49	2.7	2.0	56.3	48.7	0.3	5.7	1.3	0.3		29.0		24.3		4.7	9.9	3.3			2.7	3.9	SII
1382.95	1.9	1.3	59.2	52.0		5.2	1	0.7	0.3	29.4		25.4	0.7	3.3	8.0	3.3			0.7	4.0	SII
1383.18	8.3	0.7	51.9	47.7	0.3	3.6	0.3			29.3		23.3		6.0	9.6	3.3			3.3	3.0	SII

Table 6. Bulk mineralogy QEMSCAN data (core and cuttings samples; data presented as volume % and normalised for porosity; Tr = trace; zero values are left blank).

Well	Sample Type	Sample Depth (m)	Quartz	K-Feldspar	Plagioclase Feldspar	Heavy Minerals	Kaolinite	Chlorite	Illite/Muscovite	Dark Mica	Glauconite	Smectite	Pyrite	Calcite	Dolomite	Ankerite	Siderite	Fe-Oxides
Zema-1	core	2447.06	33.3	7.4	24.2	3.1	3.8	15.1	8.4	0.6	0.6	1.3	Tr	0.3	Tr	0.2	1.6	0.1
	core	2453.56	20.8	14.3	15.9	1.1	1.4	0.3	18.4	1.3	0.3	0.5	Tr	24.8	Tr	0.9	Tr	Tr
	core	2459.95	32.7	8.7	25.9	3.6	3.3	10.9	9.3	0.6	0.4	2.5	Tr	0.2		Tr	0.2	0.1
Ladbroke Grove-3	core	2561.00	49.0	10.2	22.7	1.0	5.8	0.1	7.9	Tr	0.1	0.1	Tr	1.5	Tr	0.5	1.1	Tr
	core	2565.67	64.1	8.5	10.2	1.5	6.3	3.0	4.0	Tr	Tr	Tr	Tr	1.3	0.4	0.2	0.3	Tr
	core	2566.58	29.2	11.9	20.4	1.2	2.7	4.4	13.3	1.6	0.3	1.0	Tr	8.8	Tr	3.3	1.9	Tr
	core	2568.63	33.6	12.1	20.2	1.6	1.3	1.3	9.8	0.7	0.4	0.9	Tr	16.3	Tr	1.5	0.3	Tr
	core	2570.85	35.8	10.0	23.4	3.0	5.6	6.8	8.0	0.7	0.2	4.5	Tr	1.4	Tr	0.4	0.1	Tr
Garvoc-1	core	1379.85	73.5	0.1	Tr	3.2	20.8	Tr	2.1	Tr	Tr		Tr	Tr	Tr	Tr	0.1	0.1
	core	1380.35	68.6	0.1	Tr	0.5	26.8	0.1	0.6	Tr	Tr	Tr	0.1	Tr	Tr	Tr	0.9	2.3
	core	1381.63	61.9	0.2	Tr	0.6	33.0	Tr	1.7	Tr	Tr	Tr	0.1	Tr		Tr	0.8	1.7
	core	1382.95	67.7	0.1	Tr	1.6	26.9	Tr	1.3	Tr	Tr		0.1	Tr		Tr	0.8	1.5
Ladbroke Grove-3	cuttings	2499	15.7	26.8	12.1	1.1	4.2	0.9	29.3	3.2	1.9	1.9	Tr	2.2	0.1	0.3	0.4	Tr
	cuttings	2502	24.7	19.4	15.7	1.5	5.0	1.4	23.7	2.3	1.3	1.7	Tr	1.1	0.1	0.4	1.6	0.1
	cuttings	2505	19.3	16.7	11.6	1.9	4.8	1.7	30.5	3.9	3.0	2.6	Tr	2.6	Tr	0.3	1.0	0.1
	cuttings	2508	28.0	7.6	28.4	2.4	6.7	0.9	16.9	0.6	1.0	1.1	Tr	1.2	Tr	0.3	4.5	0.4
Garvoc-1	cuttings	1359.41	43.8	4.2	1.1	2.1	19.2	0.5	7.5	0.2	0.6	Tr	0.1	9.4	0.6	4.9	5.1	0.7
	cuttings	1362.46	49.2	4.2	0.9	1.7	19.9	0.4	7.2	0.1	0.6	Tr	0.1	7.1	0.6	3.3	4.0	0.6
	cuttings	1365.50	44.4	3.6	1.7	1.9	22.2	0.7	6.9	0.2	0.6	Tr	0.9	6.6	0.5	3.4	5.6	0.7
	cuttings	1368.55	90.2	0.6	0.2	0.3	4.6	0.1	1.1	Tr	0.1	Tr	Tr	1.0	0.1	0.6	0.8	0.4
	cuttings	1371.60	88.3	0.6	0.4	0.3	5.9	0.2	1.2	Tr	0.1	Tr	0.1	0.9	0.1	0.4	0.8	0.7
	cuttings	1374.65	74.5	1.0	0.6	0.7	11.0	0.5	2.0	0.1	0.2	Tr	0.2	3.5	0.2	0.8	3.2	1.3
	cuttings	1386.84	68.7	2.2	2.3	1.1	9.3	0.4	4.2	0.2	0.6	0.1	0.5	3.8	0.3	1.0	4.3	1.1
	cuttings	1478.28	90.6	0.4	0.1	0.2	1.8	0.2	1.5	0.1	0.1	0.1	Tr	0.3	Tr	0.1	2.3	2.1
	cuttings	1490.47	87.5	0.6	0.2	0.2	2.8	0.4	1.9	0.1	0.1	0.2	Tr	0.2	Tr	0.1	1.8	3.8
	cuttings	1496.57	70.8	1.8	1.3	0.6	5.5	0.8	5.1	0.1	0.2	0.9	0.2	1.8	0.1	1.4	5.7	3.1

cuttings	1505.71	67.4	2.8	1.5	1.0	4.7	1.1	6.5	0.2	0.4	2.9	2.5	3.0	0.1	0.7	4.2	0.8
cuttings	1514.86	82.9	0.9	0.5	0.7	3.0	0.7	2.6	0.1	0.1	1.1	Tr	0.6	Tr	0.2	2.3	4.1

Table 7. Lithotype analysis from QEMSCAN (cuttings samples; data presented as volume %; Tr = trace; zero values are left blank). Note that cuttings at top reservoir are likely to have some caving from overlying seal.

Well	Sample Depth (m)	Stratigraphy	Fines (cuttings < 100 µm size)	Quartz grains	Feldspar grains	Heavy Minerals /Pyrite	Fe oxides	Loose Carbonate	Shells	Loose Kaolinite	Kaolinite-rich siltstone	Other Siltstone	Very Fine Grained Kaolinite-rich Sandstone	Other Very Fine Grained Sandstone	Fine-Medium Grained Kaolinite-rich Sandstone	Other Fine-Medium Grained sandstone	Siliceous Cuttings
Ladbroke Grove-3	2499	Base seal	1.9	0.1	Tr						0.1	91.6		1.7	0.1	4.6	
	2502		1.9	0.6	0.4			0.1			0.2	59.9	0.1	14.8	0.1	22.0	
	2505	Top reservoir	10.2	1.9	1.5		Tr	1.4			0.4	74.2	0.1	5.2		5.2	
	2508		13.8	4.0	5.2	0.1	Tr			0.1	2.7	36.3	4.5	13.1	2.0	18.3	
Garvoc-1	1359.41	Base seal	2.2	6.6	0.4	0.2	1.4	2.0	0.4	0.2	37.2	10.0	26.5	2.0	5.2	4.2	1.4
	1362.46		2.8	10.3	1.0		1.4	2.8	0.7	Tr	39.0	7.0	24.8	0.9	4.3	2.7	2.3
	1365.5	Top reserv.	4.3	10.4	0.9	0.9	2.6	2.6		Tr	47.6	9.5	15.1	1.6	1.1	2.4	1.0
	1368.55	Upper reservoir interval	1.3	81.4	Tr	0.1	0.1	0.2	0.2	0.2	5.0	0.9	4.8	0.4	1.6	3.5	0.4
	1371.6		1.3	79.3	0.1	Tr	0.2	0.2	0.1	1.6	7.7	2.5	1.8	0.4	1.6	3.2	
	1374.65		2.6	61.1	0.6	Tr	3.2	2.8	0.9	1.0	17.3	2.2	2.1	0.8	2.4	2.3	0.7
	1386.84		2.7	52.6	0.3	0.6	3.2	1.9	1.6	0.1	19.2	8.3	2.5	0.8	1.4	4.4	0.1
	1478.28	Lower reservoir interval	0.6	82.3			3.8	0.2		0.1	0.9	0.8	0.1		3.4	7.5	0.5
	1490.47		0.9	79.9			5.8	0.1	0.2	0.1	1.3	2.2		0.1	5.1	4.3	Tr
	1496.57		3.6	57.6		Tr	7.4	1.9		0.2	8.2	9.6	0.4	0.6	1.6	8.2	0.9
	1505.71		6.2	56.2		2.3	2.1	2.4	0.4	0.4	3.7	18.3	0.4	0.8	1.4	4.9	0.4
	1514.86	Base reserv.	2.1	70.4			4.3	0.6		Tr	2.9	5.1	0.2	0.2	3.6	10.4	0.2

Table 8. X-Ray Diffraction data (core samples; data presented as weight %; zero values, below detection limit, are left blank).

Well	Sample Depth (m)	CO_2	Quartz	Plagioclase Feldspar	Orthoclase Feldspar	Kaolinite	Chlorite	Illite/Mica	Calcite	Siderite	Laumontite
Redman-1	2827.53	Low	41.6	18.1	5.8	1.6	2.3	5.9	24.7		
	2833.15	Low	28.0	36.8	6.8	2.2	9.6	14.7	1.9		
	2841.65	Low	63.4	23.0	5.1	1.5	3.1	3.9			
Zema-1	2426.75	Low	70.7	11.7	7.6	2.1	3.8		4.2		
	2426.95	Low	67.6	11.5	7.7	2.9	7.1		3.2		
	2447.06	Low	36.7	35.6	8.4	4.3	7.6	6.4	1.0		
	2459.65	Low	15.6	26.5	10.5	3.3	4.9	12.7	26.6		
	2459.95	Low	27.8	29.9	12.0	5.4	5.8	15.2	1.5	0.7	1.7
	2465.75	Low	29.6	30.9	12.0	4.7	6.3	14.2	0.5	0.2	1.4
Ladbroke Grove-3	2508.50	Moderate	20.5	39.8	6.6	5.8	2.4	18.3		6.6	
	2508.65	Moderate	26.5	49.1	5.9	1.2	2.2	12.7		2.3	
	2523.05	Moderate	36.4	36.5	7.9	0.8	3.8	9.0	3.7	2.1	
	2523.90	Moderate	23.7	32.8	6.9	6.0	4.4	14.6	1.2	10.5	
	2524.90	Moderate	27.5	38.9	7.5	2.8	3.1	13.4	1.8	4.8	
	2557.30	Moderate	21.0	19.6	7.2		2.3	9.8	39.0	1.0	
	2561.00	Moderate	36.8	21.9	6.6		1.1	1.7	31.9		
	2572.88	Low (below GWC)	40.8	26.2	12.8	4.8	6.5	13.2			

Table 9. Oxygen and carbon isotope compositions of carbonate cements from low (Redman-1, Zema-1) and moderate CO_2 (Ladbroke Grove-3) wells. Also shown are Watson et al. (2004) values for Ladbroke Grove-1 and Ladbroke Grove-3. *Calculated fluid carbon and oxygen isotope compositions at model temperatures 80°C and 120°C. Siderite fluid carbon isotope compositions were calculated for two end member scenarios; one where HCO_3^- is the dominant aqueous carbonate species (higher pH fluid, unshaded), and the other where H_2CO_3 is the dominant aqueous carbonate species (low pH fluid, shaded).

Sample	Well	Sample Depth (m)	Carbonate	Gradient	$\delta^{13}C_{VPDB}$	$\delta^{18}O_{VSMOW}$	Model T°C	Model T°C	$\delta^{13}C$-80°C*	$\delta^{13}C$-120°C*	$\delta^{18}O$-80°C*	$\delta^{18}O$-120°C*
Watson et al. (2004)	Ladbroke Grove-1	2555	Fe dolomite		-1.4	6.8	80	120	-2.7	-2.7	-15.8	-10.8
		2582	Calcite I[W]		-11.3	3.8	80	120	-12.6	-12.6	-15.6	-11.3
	Ladbroke Grove-3	2544	Ankerite		-3.5	6.6	80	120	-4.8	-4.8	-16.0	-11.0
1965214	Ladbroke Grove-3	2506.81	Calcite II	Gas leg	-7.5	2.3	80	120	-8.8	-8.8	-17.1	-12.8
1965214R		2506.81	Calcite II		-7.5	2.2	80	120	-8.8	-8.8	-17.2	-12.9
1965219	Ladbroke Grove-3	2523.05	Calcite I	Gas leg	-12.1	2.1	80	120	-13.4	-13.4	-17.3	-13.0
1965219		2523.05	Siderite II		-2.4	7.2	80	120	-3.7	-3.7	-14.4	-9.6
1965219		2523.05	Siderite II						-7.8	-5.3		
1965226	Ladbroke Grove-3	2557.3	Calcite II	Gas leg	-6.9	1.5	80	120	-8.2	-8.2	-17.9	-13.6
1965226R		2557.3	Calcite II		-6.8	1.3	80	120	-8.1	-8.1	-18.1	-13.8
1965227	Ladbroke Grove-3	2561.0	Calcite III	Gas leg	-6.3	0.8	80	120	-7.6	-7.6	-18.6	-14.3
1965227		2561.0	Siderite II		-4.7	3.6	80	120	-6.0	-6.0	-18.0	-13.2
1965227		2561.0	Siderite II						-10.1	-7.6		
1965229	Ladbroke Grove-3	2565.67	Calcite III	Approx. GWC	-6.8	4.6	80	120	-8.1	-8.1	-14.8	-10.5
1965229		2565.67	Siderite II		-2	7.3	80	120	-3.3	-3.3	-14.3	-9.5
1965229		2565.67	Siderite II						-7.4	-4.9		
1965230	Ladbroke Grove-3	2566.58	Calcite III	Approx. GWC	-6.6	3.6	80	120	-7.9	-7.9	-15.8	-11.5
1965230		2566.58	Siderite II		-2.5	7.6	80	120	-3.8	-3.8	-14.0	-9.2
1965230		2566.58	Siderite II						-7.9	-5.4		
1965231	Ladbroke Grove-3	2570.85	Calcite II	Water leg	-6.2	4.5	80	120	-7.5	-7.5	-14.9	-10.6
1965321R		2570.85	Calcite II		-6.2	4.4	80	120	-7.5	-7.5	-15.0	-10.7
1965232	Ladbroke Grove-3	2572.88	Calcite II	Water leg	-5.2	3.7	80	120	-6.5	-6.5	-15.7	-11.4
1965232R		2572.88	Calcite II		-6.9	5.1	80	120	-8.2	-8.2	-14.3	-10.0

1965236	Redman-1	2832.09	Calcite II	Gas leg	-6.5	0.3	80	120	-7.8	-7.8	-19.1	-14.8
1965236R		2832.09	Calcite II		-6.2	0.2	80	120	-7.5	-7.5	-19.2	-14.9
1965201	Zema-1	2418.61	Calcite III	?Paleogas	-7.3	3.3	80	120	-8.6	-8.6	-16.1	-11.8
1965209	Zema-1	2453.56	Calcite II	?Near paleoGWC	-6.8	1.8	80	120	-8.1	-8.1	-17.6	-13.3

Highlights

- CO_2-related reactions have been evaluated in sandstones with high (c. 98 mol%), moderate (29-57 mol%) and low (<1 mol%) CO_2 concentrations
- Chlorite has been altered to kaolinite in sandstones exposed to moderate and high CO_2 concentrations, but is preserved in low CO_2 wells
- Virtually all detrital feldspar has reacted in the high CO_2 well but is preserved in the moderate CO_2 well
- Hylogger^{TM} has been used to investigate vertical changes in mineralogy and shows significantly impeded reactions in fine grained baffles/seals
- Precipitation of carbonate cements is associated with reservoir-seal/baffle contacts and the gas-water-contact

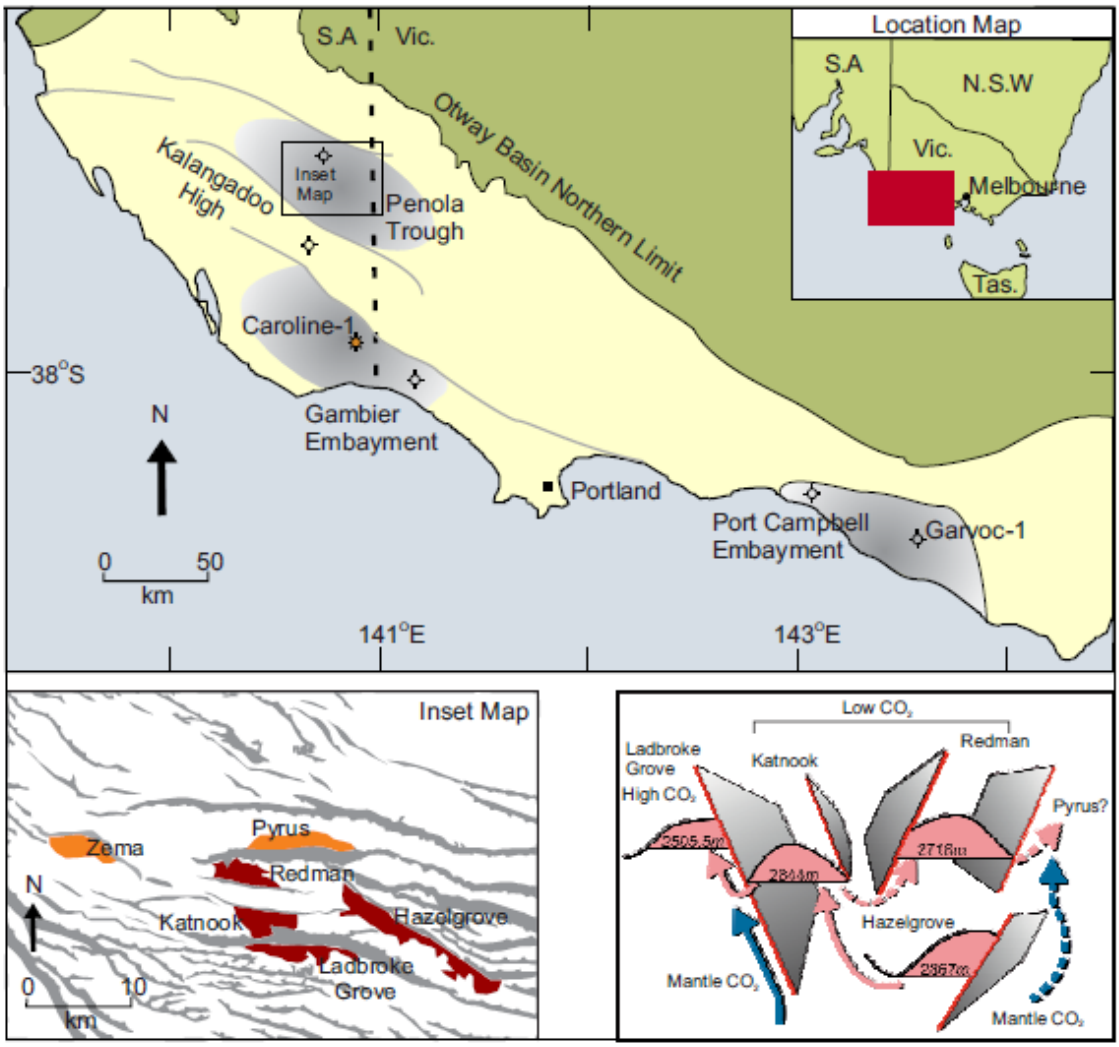

Figure 1. Otway Basin (pale yellow on map; from Watson et al., 2004a), inset map showing main faults (grey), Pretty Hill gas accumulation (red) and paleo-hydrocarbon accumulation (orange) (from Jones et al., 2000), and schematic depicting the migration pathways of deep sourced CO_2 (blue) and natural gas (pink) in the Penola Trough. Cross fault seal is interpreted to have prevented CO_2 migration into the Katnook, Redman and Hazelgrove Fields (modified from Boult et al, 2004).

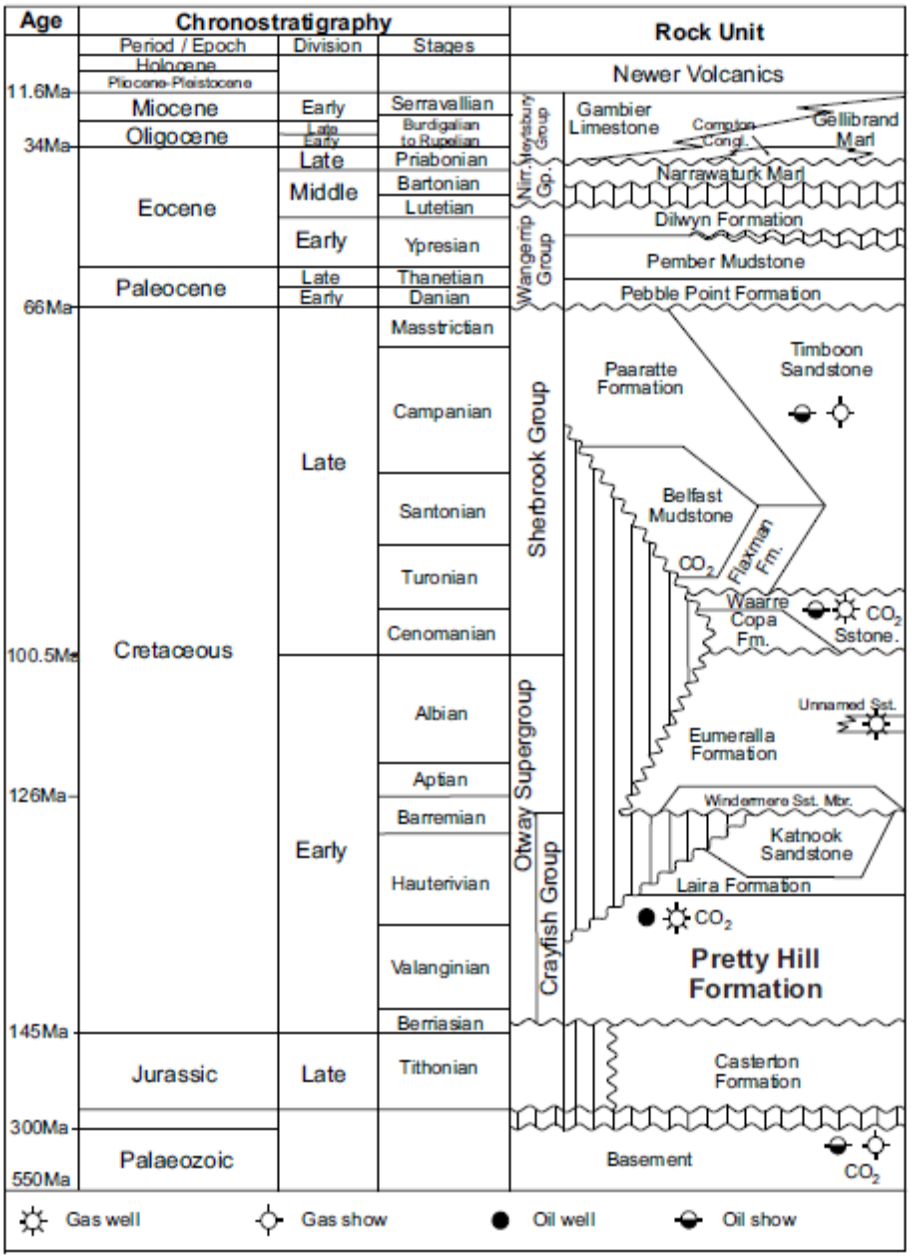

Figure 2. Generalised stratigraphic table of the Otway Basin (from Watson et al., 2004a).

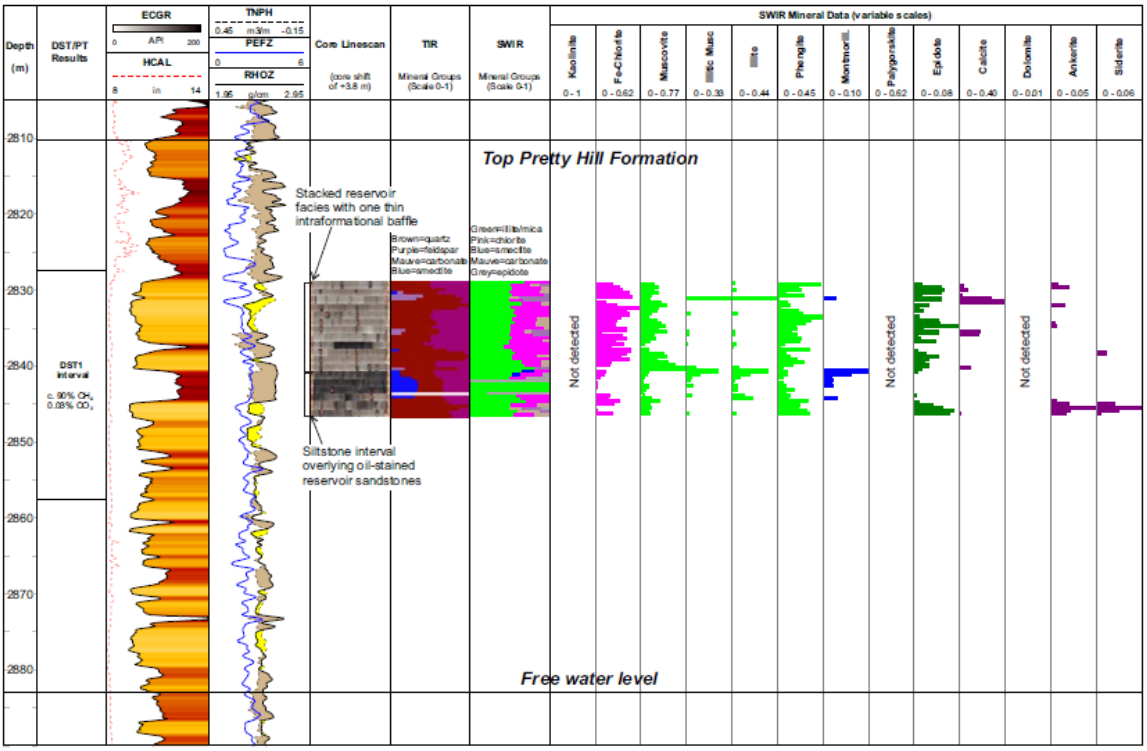

Figure 3. Summary well plot for Redman-1 showing wireline log data, core linescan (mosaiced core tray imagery output from TSG), summary TIR and SWIR mineralogy (mineral groups) and mineral assays from the TSG-core software. Hylogger mineralogy data is plotted by intensity (as measured on a scale of 0-1).

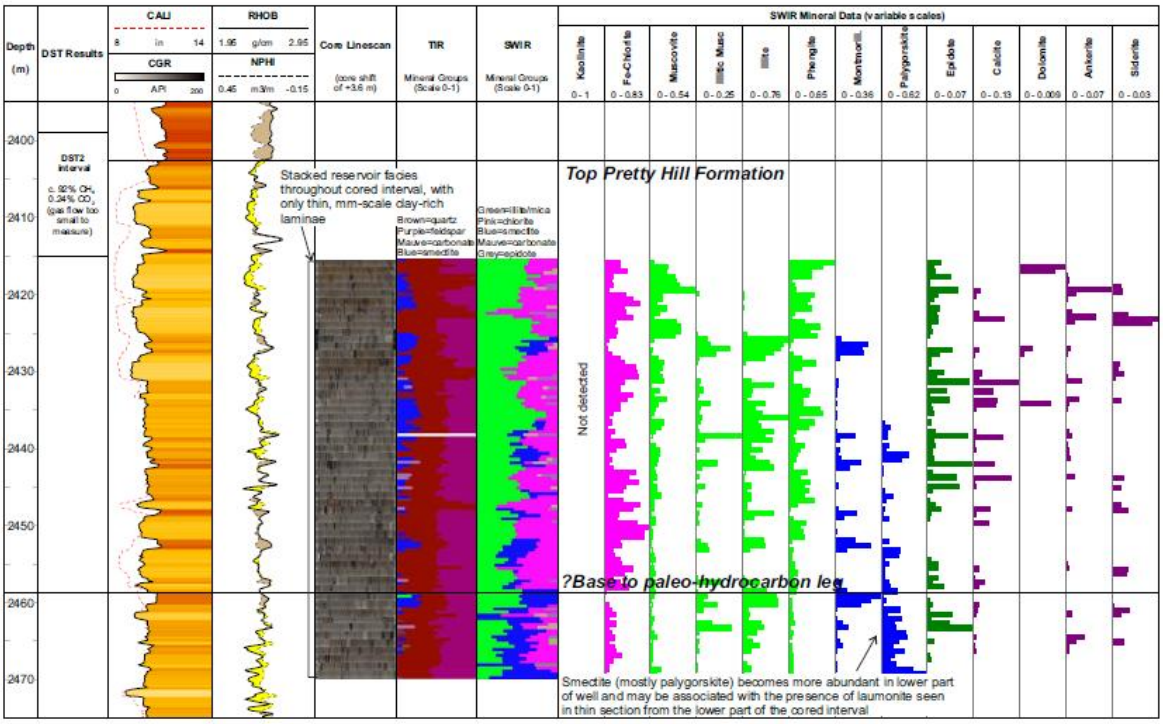

Figure 4. Summary well plot for Zema-1 showing wireline log data, core linescan (mosaiced core tray imagery output from TSG), summary TIR and SWIR mineralogy (mineral groups) and mineral assays from the TSG-core software. Hylogger mineralogy data is plotted by intensity (as measured on a scale of 0-1).

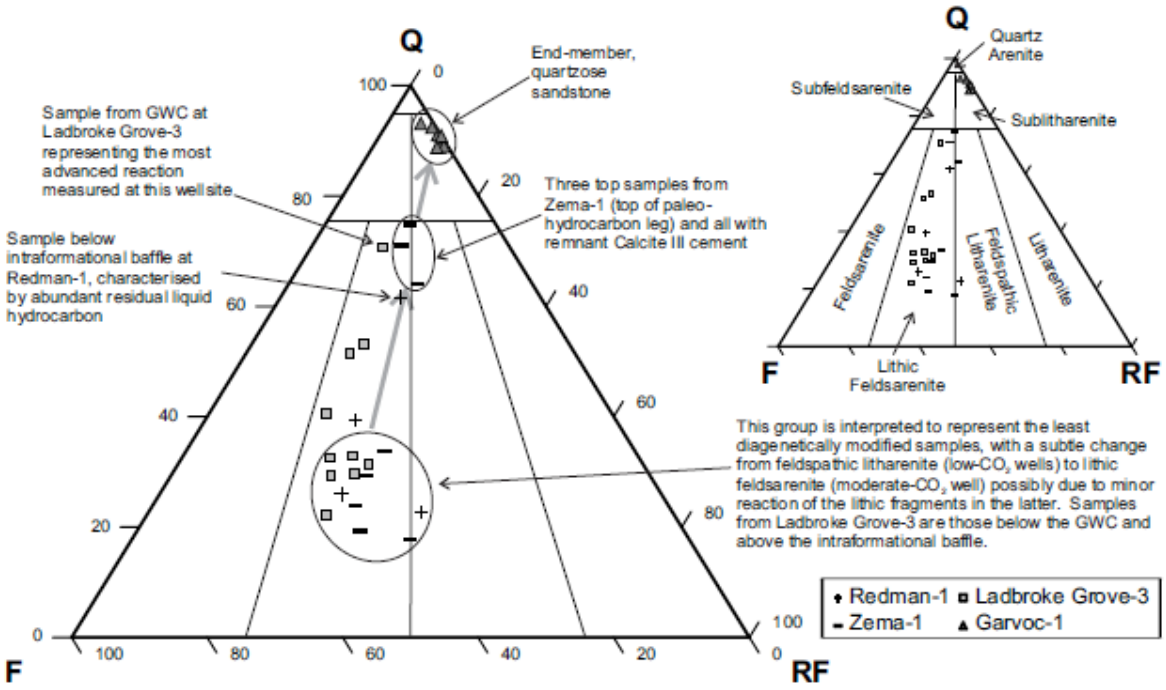

Figure 5. Ternary diagram illustrating the sandstone classification (after Folk et al., 1970) for sandstones from the Pretty Hill Formation, where Q = quartz, F = feldspar, RF = rock fragments, and the grey arrow shows the overall change in QFL due to diagenetic modification.

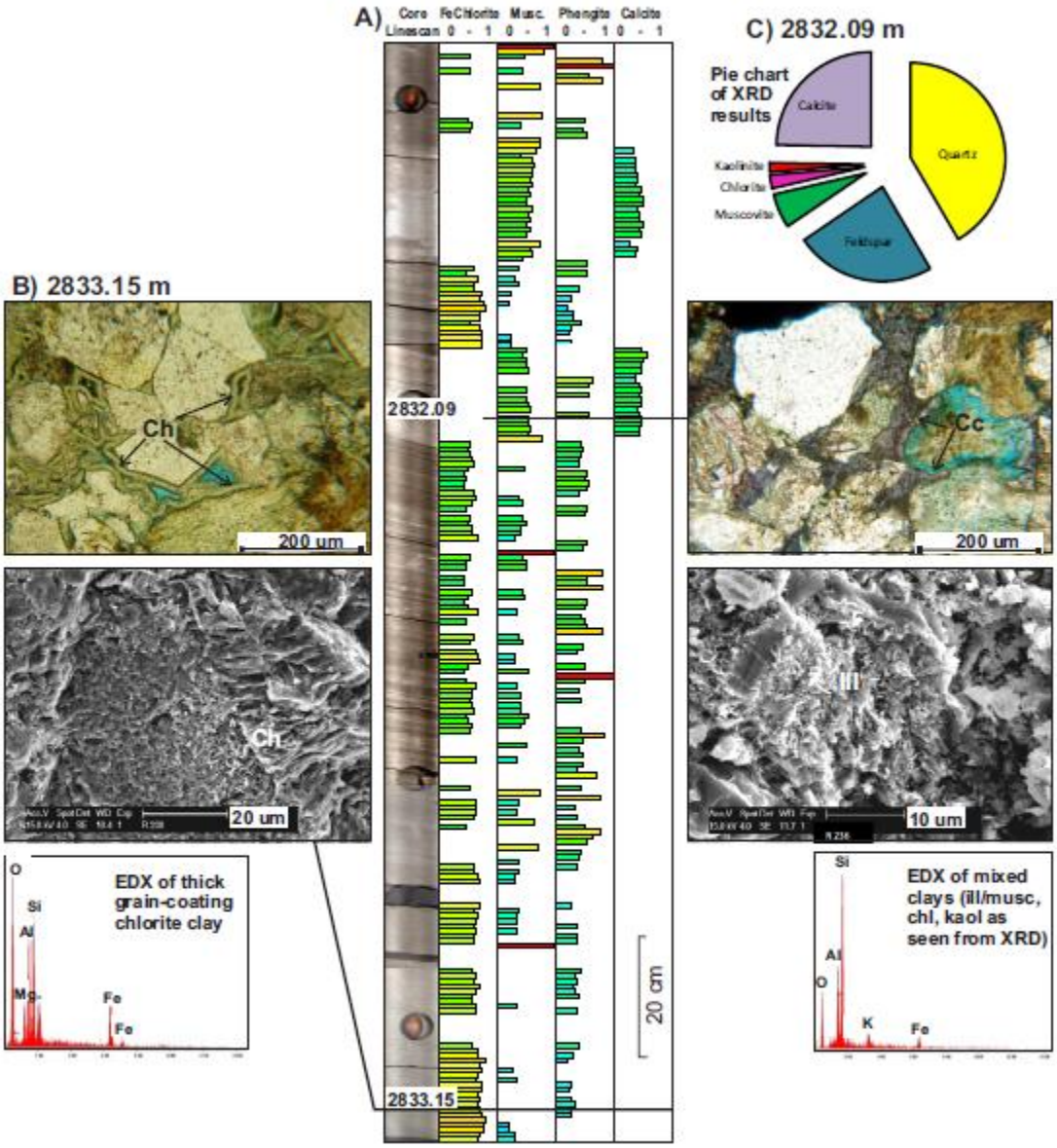

Figure 6. Integration of high-resolution Hylogger data and petrographic data, Redman-1. A) core linescan and selected mineral assays from the TSG-core software showing dominant chlorite with the exception of calcite-cemented intervals. B) and C) thin section and SEM photomicrographs, EDX clay scans, and XRD data for a chlorite sandstone (B) and a carbonate sandstone (C). Ch = grain-coating chlorite, Cc = grain-coating calcite, Ill = illitic clay. Hylogger mineralogy data is plotted as relative intensity with colours from high intensity (red), to moderate (yellow-green), to low intensity (blue); scale 0-1.

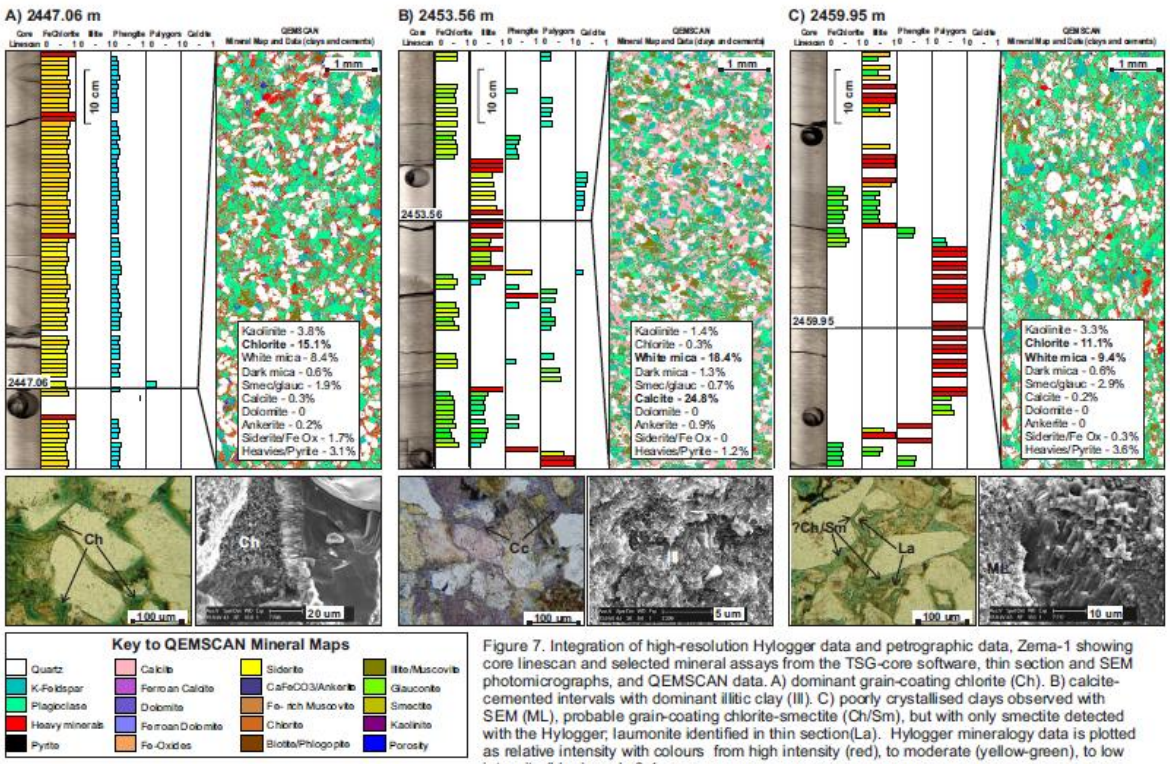

Figure 7. Integration of high-resolution Hylogger data and petrographic data, Zema-1 showing core linescan and selected mineral assays from the TSG-core software, thin section and SEM photomicrographs, and QEMSCAN data. A) dominant grain-coating chlorite (Ch). B) calcite-cemented intervals with dominant illitic clay (Ill). C) poorly crystallised clays observed with SEM (ML), probable grain-coating chlorite-smectite (Ch/Sm), but with only smectite detected with the Hylogger; laumonite identified in thin section(La). Hylogger mineralogy data is plotted as relative intensity with colours from high intensity (red), to moderate (yellow-green), to low intensity (blue); scale 0-1.

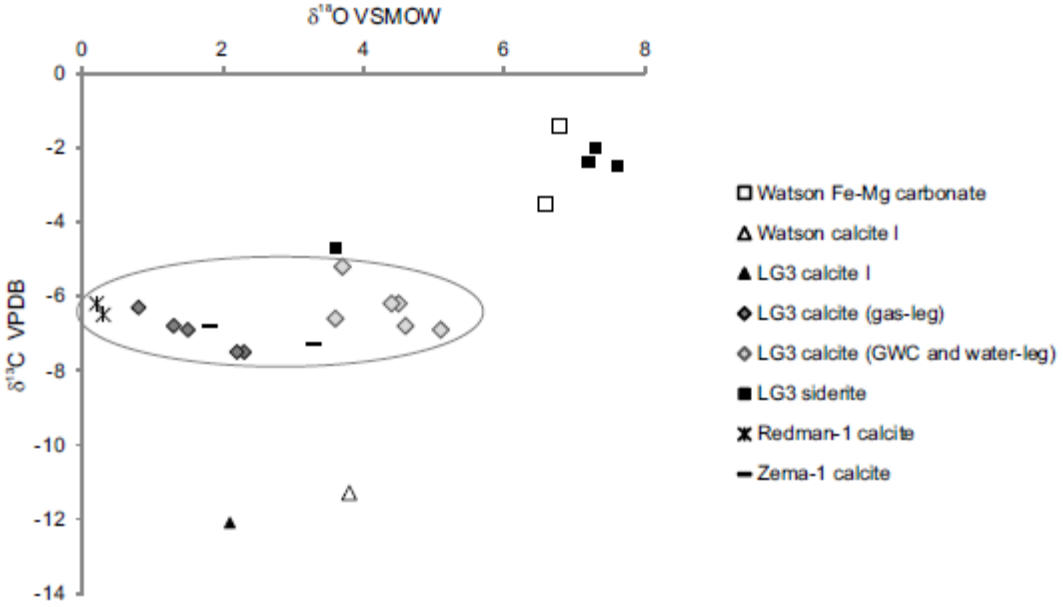

Figure 8. Oxygen and carbon isotope compositions of carbonate cements from low (Redman-1, Zema-1) and moderate CO_2 (Ladbroke Grove-3) wells. Also shown are Watson et al. (2004a) values for Ladbroke Grove-1 and Ladbroke Grove-3. Oval shape encloses the main calcite population that have similar $\delta^{13}C$ values across the low and moderate CO_2 wells; Calcite I and Fe-Mg carbonates display distinct populations.

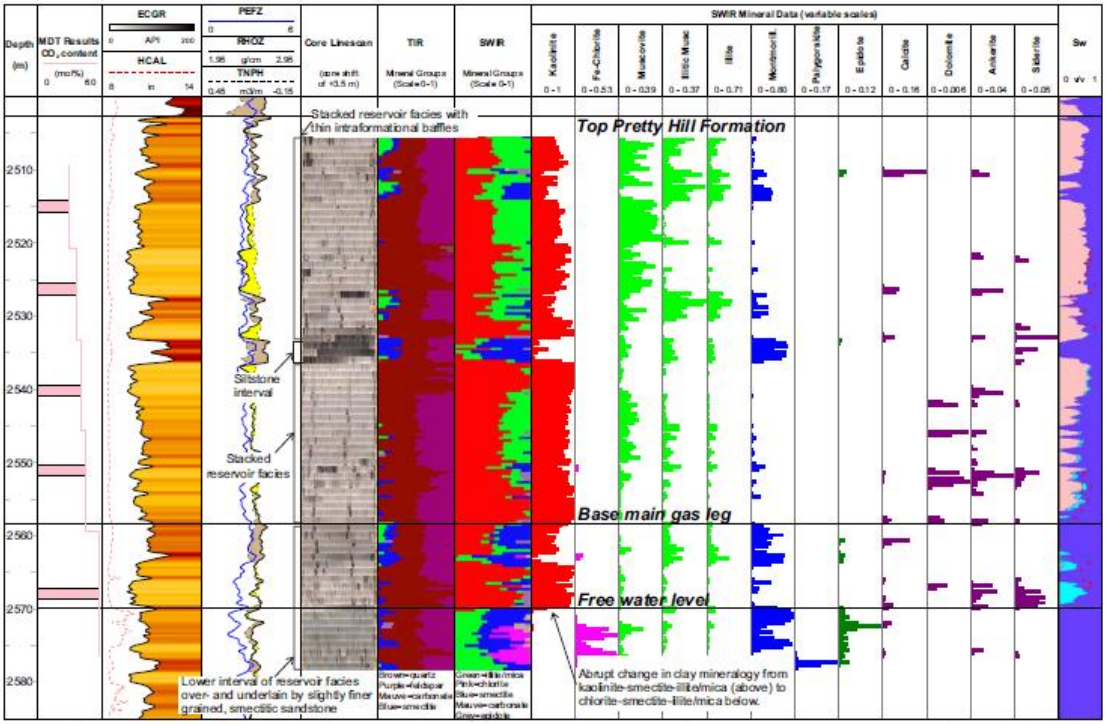

Figure 9. Summary well plot for Ladbroke Grove-3 showing wireline log data, core linescan (mosaiced core tray imagery output from TSG), summary TIR and SWIR mineralogy (mineral groups) and mineral assays from the TSG-core software, and water saturation (Sw) from Simeone and Mitchell (2001), where predicted volumes of bound water from CMR logs (dark blue) are compared with calculated Sw based on a J-function (pink/light blue, with the difference shown in light blue) and measured corEVAL capillary pressure data (red dots). Hylogger mineralogy data is plotted by intensity (as measured on a scale of 0-1).

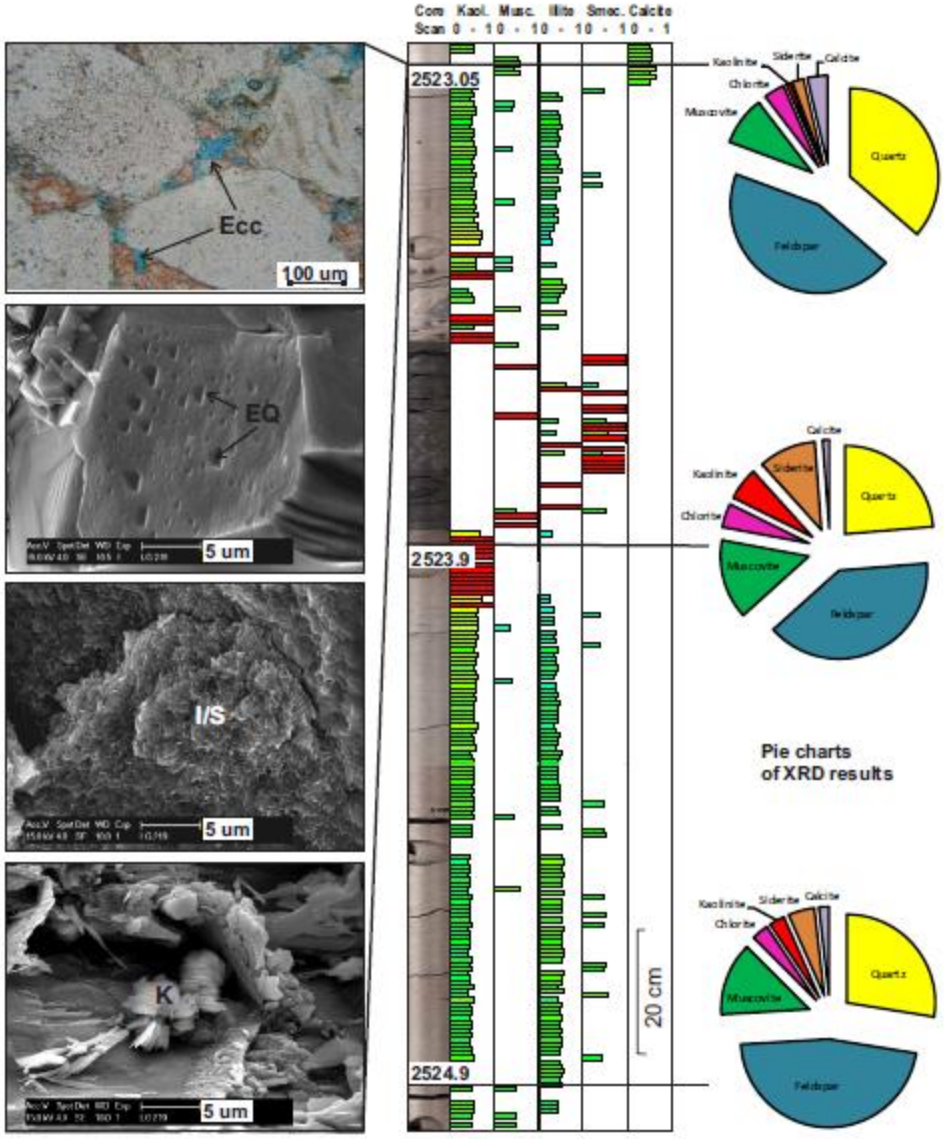

Figure 10. Integration of high-resolution Hylogger data and petrographic data, Ladbroke Grove-3 showing core linescan and selected mineral assays from the TSG-core software, thin section and SEM photomicrographs, and XRD data. Hylogger suggests an increase in kaolinite up to the base baffle (c. 2523.9 m), which is consistent with an increase in kaolinite and siderite (products of reaction) indicated by the XRD data. Hylogger suggests calcite in the 2523.05 m sample, confirmed by XRD, thin section and SEM; kaolinite is rare in this sample with dominant illitic clay. K = kaolinite, I/S = poorly crystallised illite/smectite clay, Ecc = partly etched calcite cement, EQ = etched quartz. Hylogger mineralogy data is plotted as relative intensity with colours from high intensity (red), to moderate (yellow-green), to low intensity (blue); scale 0-1.

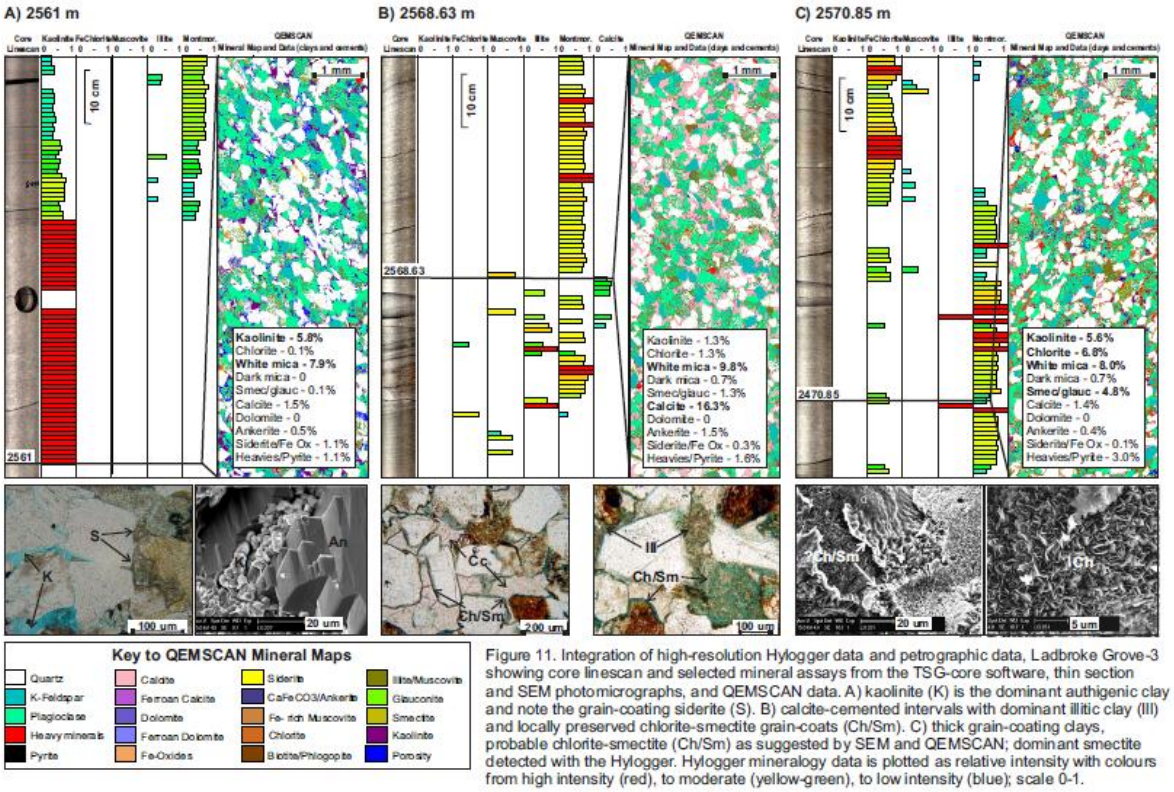

Figure 11. Integration of high-resolution Hylogger data and petrographic data, Ladbroke Grove-3 showing core linescan and selected mineral assays from the TSG-core software, thin section and SEM photomicrographs, and QEMSCAN data. A) kaolinite (K) is the dominant authigenic clay and note the grain-coating siderite (S). B) calcite-cemented intervals with dominant illitic clay (Ill) and locally preserved chlorite-smectite grain-coats (Ch/Sm). C) thick grain-coating clays, probable chlorite-smectite (Ch/Sm) as suggested by SEM and QEMSCAN; dominant smectite detected with the Hylogger. Hylogger mineralogy data is plotted as relative intensity with colours from high intensity (red), to moderate (yellow-green), to low intensity (blue); scale 0-1.

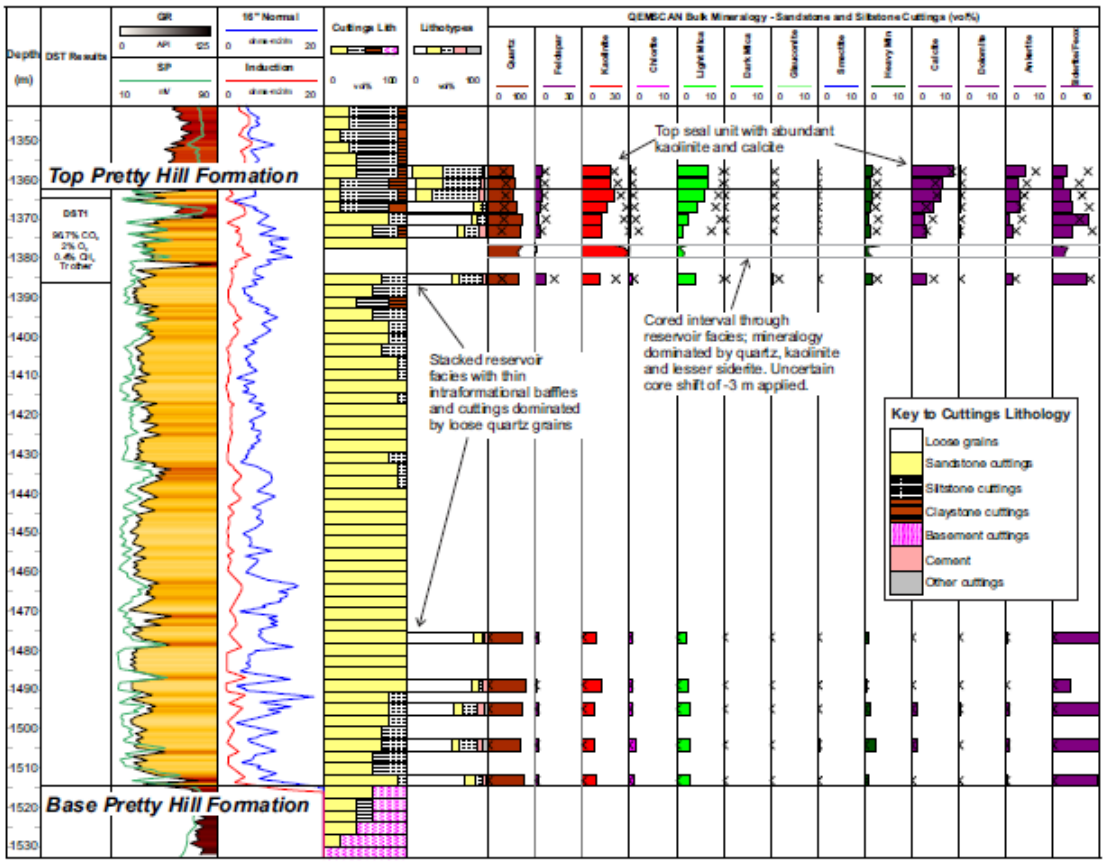

Figure 12. Summary well plot for Garvoc-1 showing wireline log data, cuttings lithology from Leslie and Sell (1968), % lithotypes from QEMSCAN and bulk mineral assays from QEMSCAN where the bars represent sandstone cuttings and the crosses represent siltstone cuttings. Note that cuttings at top reservoir are likely to have some caving from overlying seal.

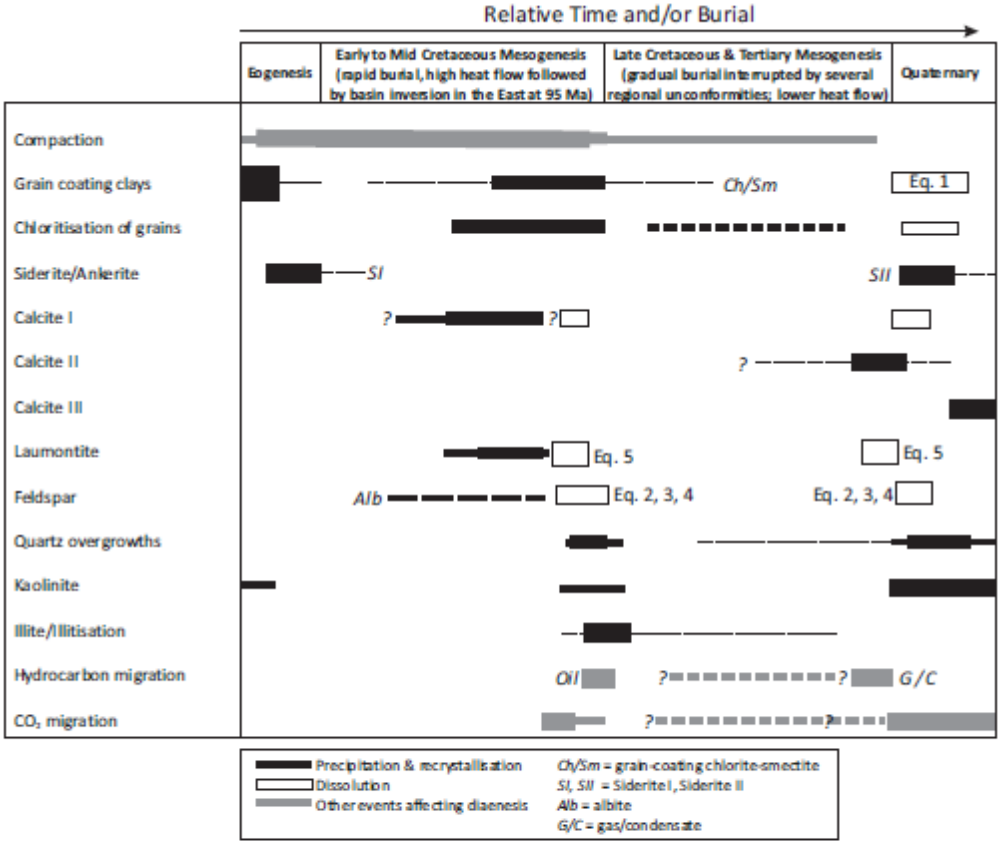

Figure 13. Diagenetic evolution of the Pretty Hill Formation relative to timing of CO_2 charge (not to scale). A mid-Cretaceous CO_2 charge is postulated, related to thermal maturation of source rocks as a result of rapid burial and high geothermal gradients throughout the early to mid Cretaceous (cf. Duddy, 1997). Further migration of both CO_2 and hydrocarbons is likely to have occurred in certain parts of the basin during the Tertiary. The main phase of CO_2 charge occurred in the Quaternary, sourced from Pleistocene to Recent volcanics (Watson, 2012). Diagenetic reactions shown here for the Quaternary will have only occurred in rocks with relatively high CO_2 contents (i.e., relatively permeable beds in the gas-leg of moderate-high CO_2 sites where CO_2 residence time is sufficiently long to promote reaction). Chlorite, feldspar and laumontite reactions (Equations 1-5) are presented in the text.